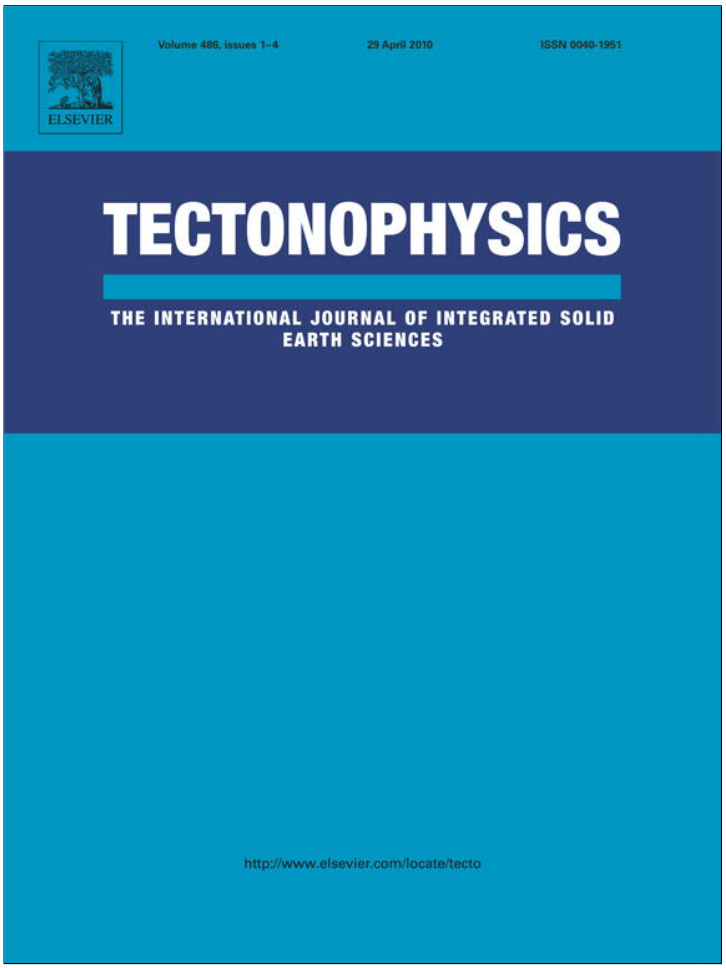

Tectonophysics 486 (2010) 81–100

Contents lists available at ScienceDirect

Tectonophysics

journal homepage: www.elsevier.com/locate/tecto

Upper mantle structure beneath the Siberian craton and surrounding areas based on regional tomographic inversion of P and PP travel times

Ivan Koulakov *, Natalia Bushenkova

Institute of Petroleum Geology and Geophysics, SB RAS, Prospekt Akademika Koptuga, 3, Novosibirsk, 630090, Russia

ARTICLE INFO

Article history:
Received 22 September 2008
Received in revised form 30 October 2009
Accepted 15 February 2010
Available online 20 February 2010

Keywords:
Seismic tomography
Upper mantle structure
Siberian craton
Mongolia

ABSTRACT

We present a model of 3D seismic anomalies in the upper mantle beneath a part of Northern Asia that includes the Siberian craton, the West Siberian Plate, the mountains framing Siberia (Altai, Sayan and Baikal) and Mongolia. We used the differential travel times of PP and P phases to investigate the deep seismic structure beneath a large part of the Siberian region, where neither stations nor earthquake distributions are sufficient to apply other body-wave tomographic schemes. To show the reliability of the results based on inversion if the PP–P residuals, we performed various tests, including: (1) tests with odd/even data; (2) synthetic tests with checkerboard and realistic patterns; and (3) inversions in other areas with clear structures. Furthermore, for the southern part of the study area, we present another model based on the Inverse Tomographic Scheme (ITS), which uses travel times recorded by worldwide stations from events located in the study area. In the overlapping areas, these two independent models are generally consistent. The main model of this study is obtained by merging the results of the PP–P and ITS schemes. This model shows a clear differentiation between the high-velocity Siberian craton and low-velocity structures beneath the mountains framing Siberia. The area of Cenozoic magmatism in Western Sayan is clearly associated with a low-velocity anomaly. At a depth of 600–700 km, this low-velocity pattern is located beneath the cratonic area, while at shallower depths, it seems to flow around the bottom of the thick craton lithosphere to the SW margin of the craton.

1. Introduction

The main objective of this study was to constrain the structure of seismic heterogeneities in the upper mantle beneath a large part of Northern Asia, including the Siberian craton, the West Siberian Plate, the mountains framing Siberia (Altai, Sayan and Baikal) and Mongolia (Fig. 1). Based on these findings and the results of other studies, in Section 8 we present our geodynamical interpretation of lithosphere–asthenosphere processes beneath selected segments of the study area.

The mantle structure beneath this area, especially its southern part, has been investigated in a number of earlier regional and global tomographic studies, which are discussed in Section 2. Many of these studies revealed some common features, such as low-velocity anomalies beneath the Sayan, the Baikal rift zone and Mongolia, as well as higher velocities beneath the Siberian craton. At the same time, one can see considerable discrepancies between all of these models, showing that seismic tomography still remains an imperfect tool. Even with dozens of tests, researchers cannot guarantee that their models adequately reflect the true structure within the Earth. This problem is mostly due to the insufficient number and/or relatively low quality of data used in these studies, which does not allow for obtaining an unambiguous solution. Furthermore, subjective factors also appear to be important. Processing of the same dataset by different authors often results at considerably different images. We believe that the comparison of various models derived from the same area, by different authors using different datasets and approaches, is very important to verify existing results. We do not pretend that our model is more sophisticated in comparison with earlier studies performed by other authors. However, it is based on another approach and uses a different selection of data. We believe that our study makes a contribution to the integrated work of others who are working in the same area. This work can strengthen our knowledge about the structure of the Earth.

This work is a continuation of our previous studies (Bushenkova et al., 2002; Koulakov, 2008), in which we constructed an upper mantle model of seismic anomalies beneath Siberia based on travel time data from the ISC catalogue (ISC, 2001). Koulakov (2008) has studied the mantle structure beneath the southern mountains framing Siberia (Altai, Sayan, Baikal and Mongolia), where quite active seismic activity is observed. In this work, an inversion was performed using the travel times from events located within the study area, which were recorded by worldwide stations at all available epicentral distances (Inverse Tomographic Scheme, ITS). In the northern part of Siberia, an insufficient number of sources and

* Corresponding author. Tel.: +7 383 3309201.
E-mail address: KoulakovIY@ipgg.nsc.ru (I. Koulakov).

0040-1951/$ – see front matter © 2010 Elsevier B.V. All rights reserved.
doi:10.1016/j.tecto.2010.02.011

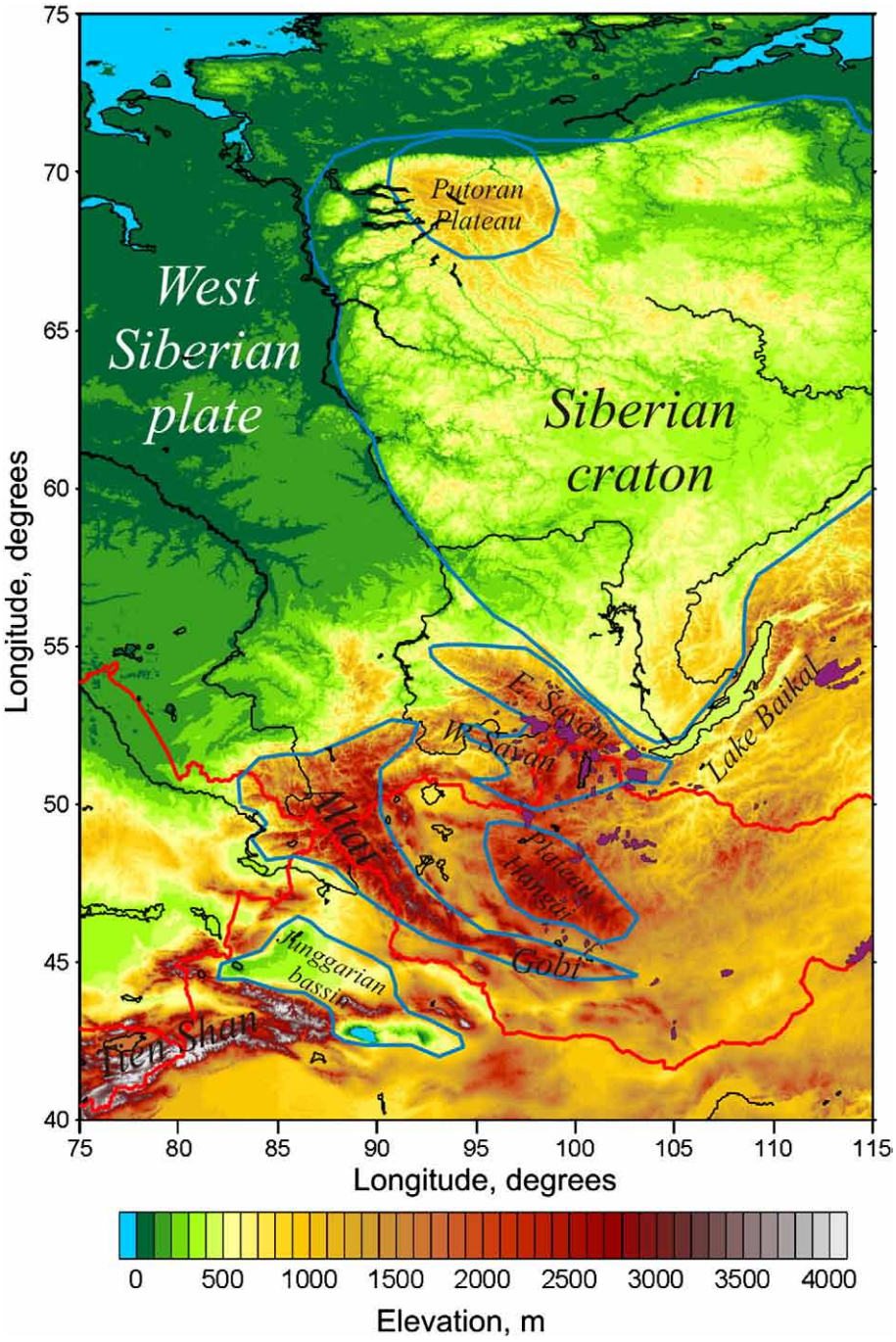

Fig. 1. Topography of the study area and the main tectonic units highlighted with blue lines. Red lines depict the state boundaries. Violet areas show fields of Cenozoic basaltic volcanism (Logachev et al., 1996). (For interpretation of the references to color in this figure legend, the reader is referred to the web version of this article.)

stations prevented the use of the ITS scheme. One of the methods that enable investigating "blank" areas is the PP–P scheme (e.g., van der Hilst and Engdahl, 1991; Vasco et al., 1995; Gorbatov et al., 2001; Bushenkova et al., 2002). This method uses differential times of teleseismic P waves and corresponding PP waves reflected from the surface at the mid-point of the ray path. Previously, we used the differential times of PP–P waves to derive a 3D model of seismic anomalies in the upper mantle beneath Siberia (Bushenkova et al., 2002). However, we continue to revise this model and to perform new inversions. The main reasons for this are:

1. In the previous work, we did not pay sufficient attention to the problem of verification. A preliminary analysis of the PP–P data shows that the quality of these data is very low. In this case, just showing the inversion results, and even demonstrating synthetic reconstructions, is not sufficient. There should be additional arguments to show the reliability of the presented patterns.
2. Since performing the last work, we have significantly modified the kernel of the tomographic algorithm. The main improvements are a more optimized parameterization with rotated grids, inversion based on the LSQR algorithm with smoothing damping and other features that will be described later.
3. In the previous version of the algorithm, the differential residuals of PP–P rays were computed without taking into account the depths of events. This caused some errors in calculating the ray paths and residuals. The data from deep events were simply

rejected, which significantly reduced the amount of data. In the new version the depths of events are taken into account.
4. We now compare the results obtained using completely different tomographic schemes, PP–P and ITS, and merge them.
5. To check the working ability of the PP–P scheme, we have performed the inversion in an area with clear deep structure, in the Ryukyu Arc (Western Pacific), where the presence of the subducted Philippine slab is indisputable.

2. Previous tomographic studies in Siberia and surrounding areas

The northern part of the study region includes stable areas of the Siberian craton and West Siberian Plate, while the southern part corresponds to tectonically active orogenic areas of the Altai, Sayan, Baikal, Hangay and Eastern Tien Shan (Fig. 1). The study region is a rather complicated area to investigate. Very large areas with low populations and difficult climate conditions make it impossible to install dense networks of seismic stations. Furthermore, a considerable part of this area is aseismic, which prevents using some common and efficient tomographic schemes. Performing a few regional projects with the use of active and passive observation schemes does not help to cover the entire area. All of the regional models constructed for this area suffer from insufficient data quality and quantity. Therefore, they are often not consistent with each other. In these conditions, a special problem is to single out more or less robust features (at least at a qualitative level) that are visible in most observations.

Regional investigations of the southern part of the study area have been performed in a number of tomographic studies since the seventies and eighties. The first regional models of Central Asia, which comprises Southern Siberia and Mongolia, were based on different data types, such as body waves (e.g., Alekseev et al., 1971), *Pn* and *Sn* travel times (e.g., Barazangi and Ni, 1982; Ni and Barazangi, 1983) and surface waves (e.g., Pines et al., 1980; Gobarenko and Yanovskaya, 1983; Brandon and Romanowicz, 1986). These pioneer studies were very important for developing theoretical and practical aspects of tomographic approaches used today. However, the results of these studies provided too low spatial resolution, and in some cases the anomalies in different models did not fit each other.

Better resolution and consistency for Northern and Central Asia was achieved in later studies, which were based on surface-wave tomography (Wu and Levshin, 1994; Wu et al., 1997; Ritzwoller and Levshin, 1998; Villasenor et al., 2001), *Pn* and *Sn* phases (Ritzwoller et al., 2002), joint analyses of S body waves and surface waves (Friederich, 2003) and P body waves (Koulakov et al., 2002; Koulakov, 2008). These models are generally consistent with P-velocity global models (e.g., Bijwaard et al. (1998), van der Hilst et al., 1997). Gorbatov et al. (2001) discussed the structure beneath Russia when they presented their global tomographic model, which was based on 3D ray tracing and used PP phases. For the study area, they revealed a high velocity beneath the Siberian craton and a low velocity beneath the West Siberian Plate. At a depth of about 450 km, beneath the southern part of the Siberian craton, they observed lower velocities, which is consistent with Koulakov (2008). Fukao et al. (2003) also discussed the mantle structure beneath the northern part of Asia, as part of a global model. They used self-picked PP phases, whose high quality was supported by a variance reduction of more than 60%. At the same time, the number of PP data was significantly smaller than in the ISC catalogue, resulting in lower resolution in areas with an insufficient number of rays. As in Gorbatov et al. (2001), this model showed a high velocity beneath the Siberian craton, but the resolved sizes of patterns beneath the northern parts of Eurasia were rather large and were comparable with the size of the craton. Similar features were found in another recent global model by Li et al. (2008) which also used PP–P differential times. At a qualitative level, all of these models revealed the same features for the southern part of the study area. These include the low-velocity pattern centered in the southern part of the Baikal rift zone, which surrounds a high-velocity anomaly beneath the Siberian craton.

In contrast to the numerous regional studies covering the southern part of the study area, the deep structure beneath the Siberian craton and West Siberian Plate has not been well investigated. Conventional regional and global tomographic schemes, based on travel times of refracted body waves, do not provide any information about the northern part of the study area. This is due to an insufficient number of seismic sources and stations. At the same time, the investigation of deep structures beneath these stable areas is also a matter of great importance. Several large-scale tectonic events have happened within Northern Siberia. The largest tectonic element is the Siberian Traps, which form a large igneous province in Siberia and cover the largest part of the Siberian craton (e.g., Zolotukhin and Al'Mukhamedov, 1988). This massive eruptive event spanned the Permian–Triassic boundary, about 251 to 250 million years ago, and was essentially coincident with the Permian–Triassic extinction event, in what was one of the largest known volcanic events of the last 500 million years. Extensive subcrops of basalt also occurred beneath the West Siberian Plate (e.g., Reichow et al., 2002; Surkov, 2002), beneath the Yenesei–Khatanga Trough and beneath the Kara Sea. Sporadic outcrops of Permo-Triassic basalt occurred also in the Urals and in the Kuznetsk Basin (Reichow et al., 2005). The existence of other more recent manifestations of intra-plate magmatism is a clear indicator of active processes beneath Northern Siberia that have lasted throughout geological history. Seismic models beneath these stable areas would help in understanding the origin of such activity.

Some information about the lithosphere and mantle structures beneath Northern Siberia is based on several transcontinental transects that used nuclear explosions as powerful sources of seismic signals (e.g., Pavlenkova et al., 1996; Egorkin, 1998; Morozova et al., 1999). However, the distribution of 2D profiles is too sparse to be integrated into one regional model. Data on all available deep seismic sounding (DSS) profiles were combined with potential fields by Surkov and Lotyshev (1989). Their work resulted in maps of crustal thickness and crystalline basement depth beneath the West Siberian Plate (WSP) and Siberian craton.

The 3D deep structure beneath such “blank” areas is investigated based on surface waves (e.g., Villasenor et al., 2001; Friederich, 2003) or the reflected phases of PP and SS body waves (e.g., Gorbatov et al., 2001; Fukao et al., 2003; Li et al., 2008). A regional tomographic model beneath the northern part of the study region has also been constructed by Bushenkova et al. (2002), with the use of PP–P data from the ISC catalogue.

There have also been some smaller scale tomography studies in the study area, which used data from temporary and permanent networks. These works provided important information about the mantle structure of this area. Most of the experiments were performed in the Baikal rift zone. Combined data from global and regional networks were used in Petit et al. (1998) and Koulakov (1999). Jakovlev et al. (2007) used *Pn* and *Sn* data, recorded by permanent regional networks in the Baikal area, to estimate the Moho depth and to map seismic heterogeneities in the uppermost mantle. The results of these studies, as well as the model by Koulakov (2008), are in general correlation with the teleseismic tomography performed by Zhao et al. (2006), which was based on the data of temporary networks in the Baikal rift zone. Recently, results were obtained for a S–N profile that crosses Mongolia and passes through the Hangay dome (Tiberi et al., 2008). Reported residuals of teleseismic rays along this profile fit with most of the regional models mentioned above.

The structure obtained beneath Southern Siberia from most regional and global studies has revealed some important features for geodynamic interpretation. In particular, at depths down to 200 km, the southern part of the Siberian craton is surrounded by a

prominent low-velocity anomaly. The maximum of this anomaly coincides with a distribution of Cenozoic magmatism and the Baikal rift zone (e.g., Logachev et al., 1996; Logachev, 2005). Koulakov (2008) suggested that a flow of hotter material ascends beneath the Siberian craton up to a depth of 200–300 km, where it meets the bottom of the lithosphere. This material then flows up around the craton and causes manifestations of basaltic magmatism along its southern perimeter. For the Baikal area, a similar concept was proposed earlier and was based on smaller scale regional tomographic studies by Petit et al. (1998), Koulakov (1999), Zhao et al. (2006), Lebedev et al. (2006) and others.

3. Inversion according to the PP–P scheme: data, algorithm and results

The general idea of using reflections from surface phases to investigate areas with poor source and receiver coverage was proposed in the 1980s and 90s (e.g., Darragh, 1985; Woodward and Masters, 1991; van der Hilst and Engdahl, 1991). Phases of reflected PP and SS waves have been used in several regional and global tomographic studies. On a qualitative level, SS–S residuals were used to evaluate the anomalies beneath Tibet by Woodward and Molnar (1995). The tomographic inversion of this data set for the same region was performed by Dricker and Roecker (1994, 2002). Various phases of reflected S waves (e.g., SS and SSS) have been used to obtain a regional model beneath the USA and Northern Atlantic (Grand, 1994), as well as a global model (Grand et al., 1997). The arrival times of several compression and shear phases, including PP and SS times, were used by Vasco et al. (1995) and Vasco and Johnson (1998) to infer the global Earth's three-dimensional structure. Widiyantoro et al. (2000) and Gorbatov et al. (2001) used travel times of PP rays to improve their global models in areas with insufficient data coverage. Fukao et al. (2003) supplemented the dataset with self-selected, high quality PP phases and constructed another global model. One of the most recent global models by Li et al. (2008) also used the PP–P differential times together with many other phases.

We use the basic principle of the PP–P regional algorithm, which is described in detail by Bushenkova et al. (2002). This scheme uses PP and P (or SS–S) rays that correspond to same source–receiver pairs. Subtracting the PP and P travel times allows us to avoid any effects related to the uncertainty of the source location and features in the source and receiver areas. Tomographic inversion uses the residuals between differential times observed and computed in the reference model. Assuming that the velocity anomalies in the lower mantle are much weaker than in the upper mantle, these differential residuals are mostly related to the structure in the area beneath the bounce point of the PP ray. Thus, using PP rays with reflection points located inside the study area, we can retrieve relevant information about deep seismic structures beneath the study area.

We have also tried to use pairs of SS–S rays. In the literature, studies based on SS rays are quite frequent (e.g., Grand et al., 1997; Dricker and Roecker, 2002). However, our attempt failed. The inversion of SS–S data did not reveal any coherent structure. This conclusion is based on the results of odd/even tests and on reconstruction in a testing area (Ryukyu Arc, Western Pacific), which is considered in Section 4. One of the major reasons for this is that the error of selecting the S phase is much larger than for the P phase. Therefore, differential SS–S contains significant errors for both SS and S picks, while in the case of PP–P times, the major error is only due to PP picking. Furthermore, the number of SS–S pairs in the ISC catalogue (ISC, 2001) is considerably smaller than that of PP–P, which may be another reason for the lower robustness of results based on SS–S data.

Fig. 2 shows the bounce points corresponding to all PP–P pairs from the ISC catalogue for the years 1964–2001 (International Seismological Centre, 2001) for the entire Earth and for the study area. This figure demonstrates that the Siberian region has one of the densest distributions of PP bounce points on Earth. However, inside the area the density of points is heterogeneous. The inversion was performed separately in five overlapping circular windows that were 9° in radius, as shown in the right plot in Fig. 2. The number of bounce points varied in different windows from around 3000 to 8000.

The reason for using the inversion in separate windows is discussed in Koulakov et al. (2002) and Koulakov and Sobolev (2006). These studies showed that, for investigating the upper mantle (approximately 700 km in depth), the optimal diameter of the study area is 1500–2000 km. This provides the best ray configurations, enabling a reduction in the effect of lower mantle heterogeneities. In addition, the comparison of results from overlapping windows is another test that can be used to check the stability of the inversion. In particular, if an anomaly is located near the margin of one of the windows, the neighboring windows can be checked to see if the anomaly is significant or if it is a marginal artifact. Furthermore, overlapping of neighboring windows has a smoothing effect on the results and helps to stabilize the inversion.

In the present study, the data selection from the ISC catalogue for the years 1964–2001 (ISC, 2001) had only two requirements: (1) there should be both PP and P rays corresponding to the same source–receiver pair and (2) the reflection point of the PP ray should be inside the study area. We did not apply a limitation for the source depths, as were used in Bushenkova et al. (2002). This increased the number of data utilized, compared to the previous study. For the study area we almost did not have any PP–P pairs corresponding to source–receiver distances of less than 30° that determine natural distance truncation of data. All the PP travel times were corrected for topography.

Reference times for PP and P rays were obtained by bilinear interpolation, based on a reference table computed at a preliminary stage. This table contains travel times, dip angles and maximal depths of rays, depending on epicentral distances and the source depth. These parameters were computed based on a 1D spherical model of the Earth AK135 (Kennett et al., 1995) and using analytical formulas of ray tracing from Nolet (1981). Distributions of differential residuals of the PP–P phases with respect to epicentral distances for the entire ISC databank are shown in Fig. 3. It can be seen that, for some epicentral distances, there is a strong bias. We did not explore the nature of this effect. We suppose that for large epicentral distances it may be due to an inappropriate reference model, which was constructed mostly from minimizing misfits of the travel times of refracted rays and not the PP rays. For distances of around 20° the bias reaches 5 s and it may have to be attributed to some systematic reading errors of the P and/or PP arrivals due, for example, to the Moho discontinuities. It is possible that reported PP phases are in fact the Pg waves with crustal velocity that may explain 5 s of delay at 20° distance. In our inversion, we constructed the relative anomalies based mostly on teleseismic rays with large distances. For the Siberian region we practically do not have any examples of a source–receiver pair at distance of less than 30° having middle point inside the study area. It is confessed that the teleseismic rays cannot provide stable values for the absolute velocities. Therefore, we can bias the residuals with respect to their average value, which is roughly equivalent to the bias of the absolute velocities. This regular bias of the residuals was taken into account by adding corrections, which are shown by the white curve in Fig. 3 and were constructed as a smoothed average value of the observed residuals. After adding the corrections, we took into consideration the pairs of PP–P rays with residuals less than 4 s.

Parameterization of the seismic velocity distributions was performed based on the algorithm developed by Koulakov et al. (2002) and Koulakov and Sobolev (2006). A certain number of nodes were distributed within the study volume, according to the ray sampling. In this study, the nodes were placed at 14 horizontal levels ranging from 50 to 700 km depth and with an interval of 50 km. Nodes at each

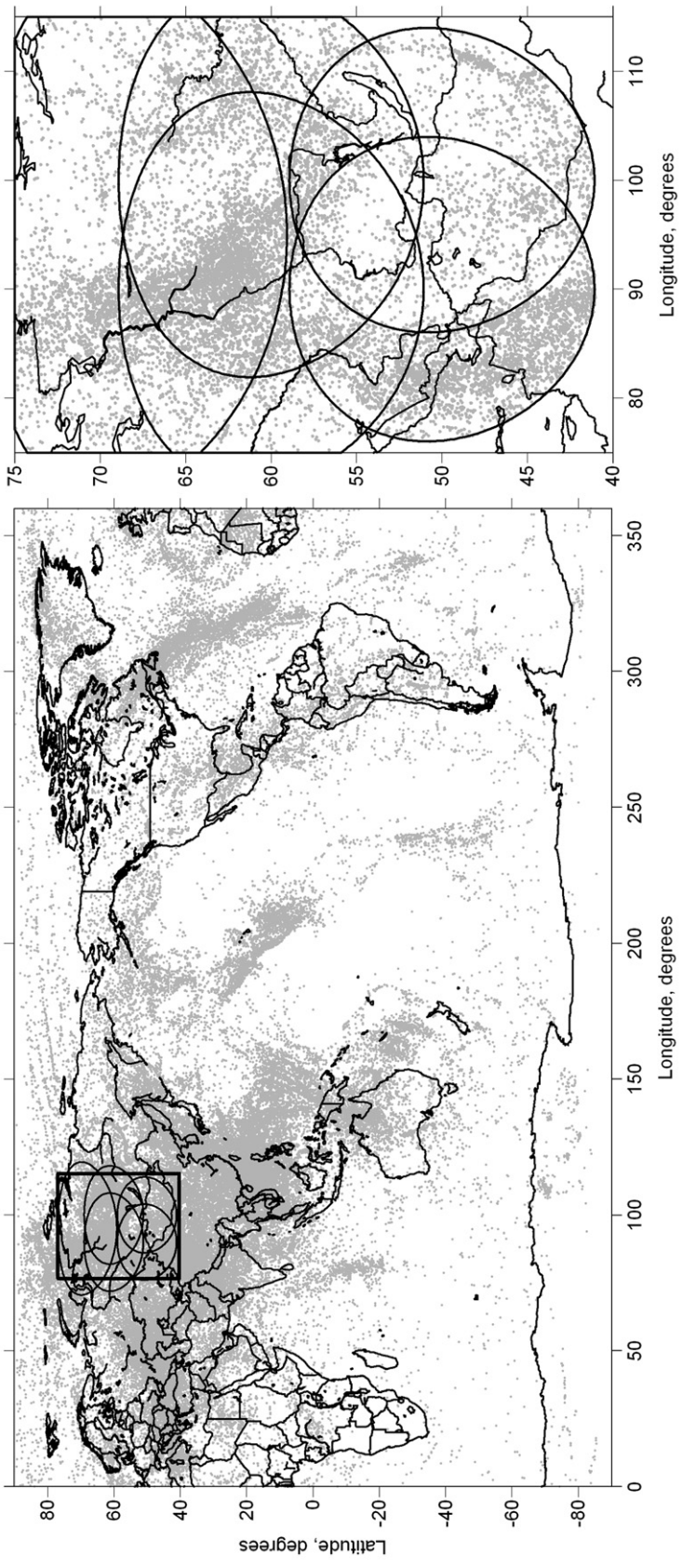

Fig. 2. Left: global map of the bounce points of PP rays (grey dots) reported in the ISC catalogue. Right: bounce points corresponding to the data selected for this study. Five ellipses indicate circular windows where separate inversions were performed.

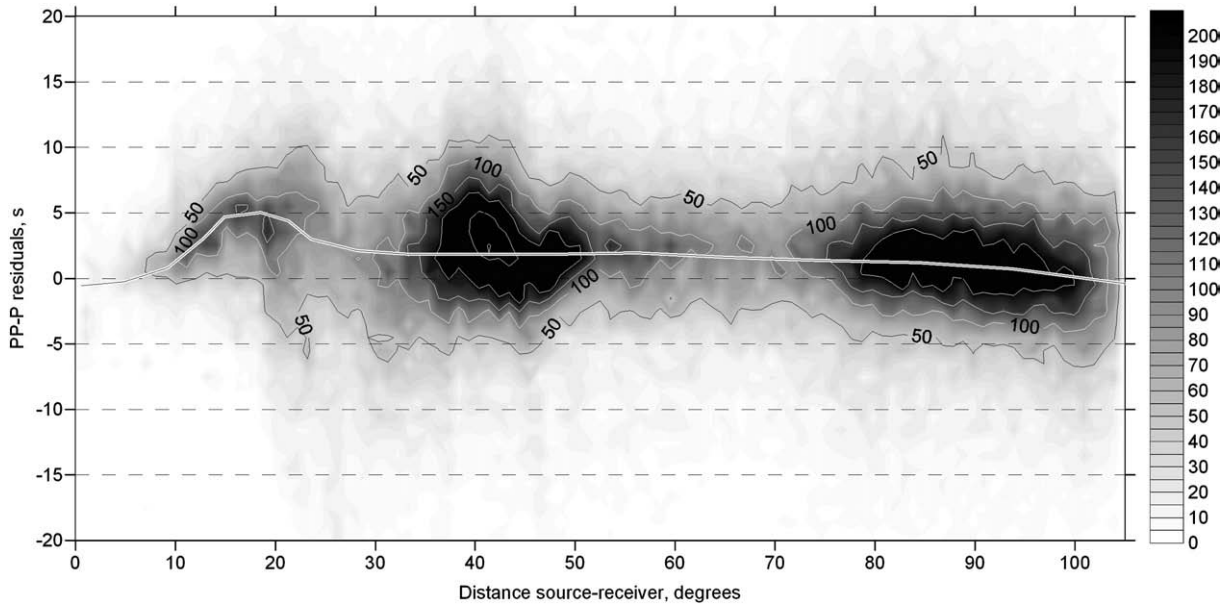

Fig. 3. Distribution of the differential PP–P residuals in the global ISC catalogue. Grades of grey indicate number of picks in the intervals of 1° of epicentral distance by 0.5 s of time. White line indicates the reference level which was used to compute the residuals in this study.

depth level were installed in parallel lines. In each line, the node spacing was inversely proportional to the ray density (summary of ray length in a unit volume). However, a minimal spacing ($dS^{min} = 50$ km) was set to avoid excessive concentrations of nodes. The number of nodes in each circular area varied from 2600 to 3900, depending on the number of data in a window. In this parameterization, eight nodes forming 3D trapezoid (two nodes on each of four parallel lines in two depth levels) controlled each point of the study area. The velocity distribution was approximated using bilinear interpolation. The proposed parameterization had a preconditioned orientation of parallel lines with nodes that may have affected the result. To minimize this effect, we performed separate inversions for four differently oriented grids (at 0°, 22°, 45° and 67°). Summation of the resulting models removed most of the artifacts related to grid orientation.

We define node spacing much smaller than the expected size of resolved patterns (which can be a-posteriori checked by checkerboard test). In this case, node distribution does not affect the shape of the resulting anomalies. The resolution in our algorithm is merely controlled by inversion regularization parameters (damping and smoothing) and appears to be independent of grid configuration.

The first derivative matrix *A*, which reflects the effect of velocity variations at each parameterization node on the travel time of each ray, was computed along the ray path constructed in the 1D spherical model. The resulting matrix was inverted using the LSQR method (Paige and Saunders, 1982; van der Sluis and van der Vorst 1987). An additional matrix block controlled smoothing of the resulting velocity anomalies. Each line in this block contained two non-zero elements having opposite signs, corresponding to neighboring nodes in the model. Increasing weights of these elements produced a smoothing effect upon the resulting anomalies. The variance reduction for PP–P residual times after inversion was quite low (15–20%, depending on the window), due to the low ratio of signal/noise in the data. Therefore, the reliability of such results must be thoroughly checked.

Fig. 4 presents four horizontal sections of the resulting 3D velocity anomalies derived from inverting the PP–P data. This model was obtained based on the averaging of 20 separate inversion results (four grids with orientations at 0°, 22°, 45° and 67° in each of five circular windows). Taking into account the very low data quality, we do not pretend that the presented patterns reveal the true amplitudes and shapes of real structures in the Earth. The main purpose of this study was not to show these types of results but to provide arguments about the degree to which these structures are trustworthy and in which parts of the study area we can believe them. Therefore, before discussing the interpretation of this model, we present several tests that reveal the unbiased reliability limits of the results.

4. Verification of the results based on the PP–P scheme

Any tomographic inversion guarantees obtaining some solution. However, the key problem of such studies is not in showing the resulting maps and cross sections, but in providing arguments that this solution reflects real structures in the Earth. The problem of verification is especially important for noisy datasets, as used in this study. The traditional testing approaches, such as showing the resolution matrix or checkerboard tests, are not sufficient for this case. They are mostly oriented towards revealing the resolution characteristics related to the matrix structure and ray configuration. At the same time, in the case of noisy data, these factors become less important than the artifacts related to errors in data.

First of all, to make sure that the PP–P scheme works in the general case, it should be applied for an area where the structure is clear and well known from other methods. One of the best candidates for such testing is an area of subduction of the Philippine plate between Japan and Taiwan along the Riukyu arc. Here, the shape of the subducted slab is clearly marked by deep seismicity in the Benioff zone. A high-velocity anomaly related to the slab is clearly visible in global (e.g., Bijwaard et al., 1998, right map in Fig. 5) and regional tomographic models. The central map in Fig. 5 shows our results based on the ITS scheme using the same algorithm as considered in Section 5 of this paper. The density of bounce points of the PP rays in this area is of the same order as for the northern part of the Siberian region. Thus, for the PP–P scheme, the observation conditions are similar in these two areas. Results of inversion of PP–P data for the Riukyu arc are shown in the left map of Fig. 5. The model based on PP–P data cannot compete in reconstruction quality with the global and regional models based on the events in the subduction area. It should be noted that the typical thickness of the slab is about 100 km and the resolution of the PP–P scheme is estimated for Siberia at 300–600 km. Thus, the slab is too thin to be resolved with the PP–P scheme. At the same time, on a qualitative level, the position of the slab-related high-velocity anomaly is recovered correctly. From the comparison of

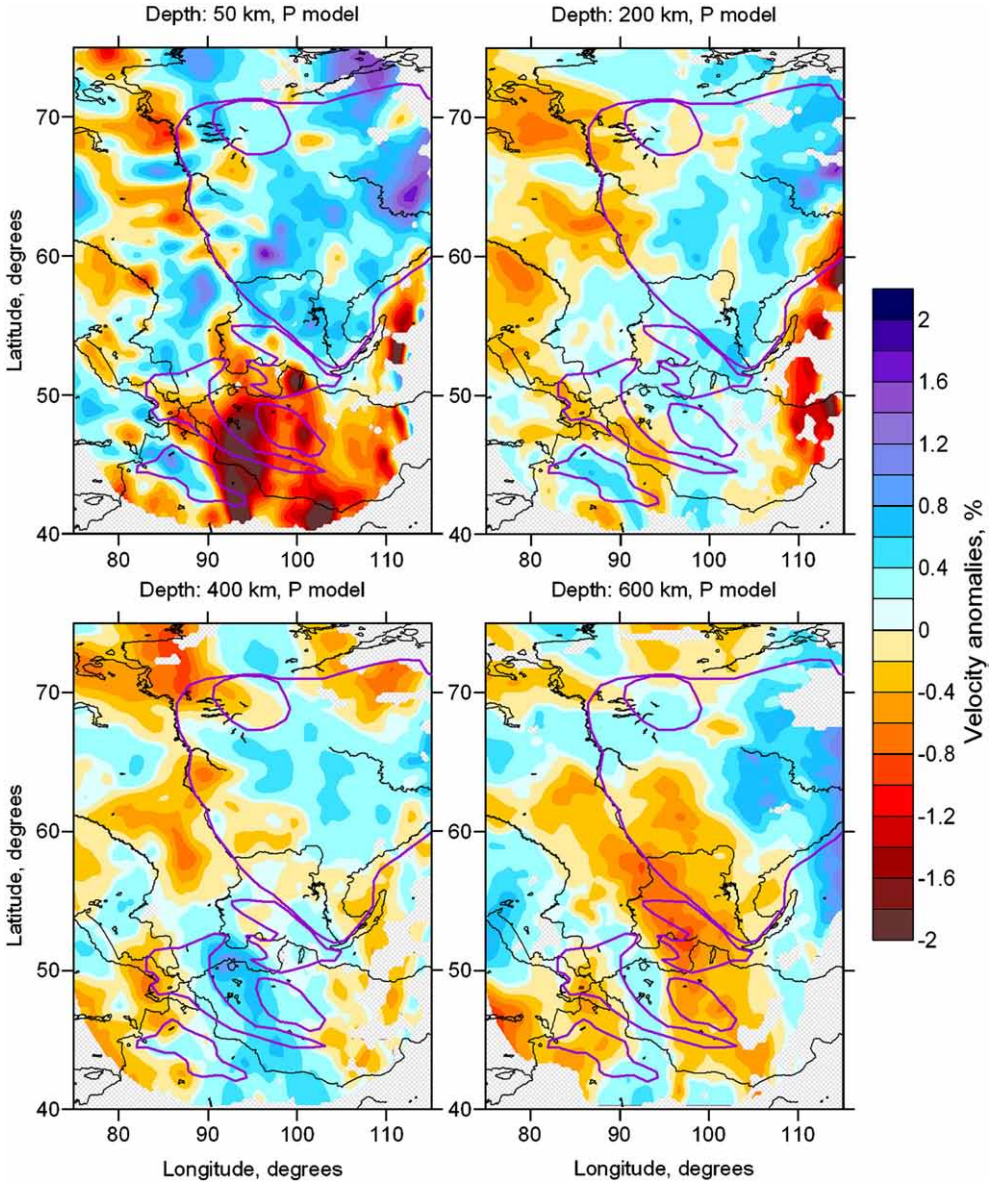

Fig. 4. Horizontal sections with P-velocity anomalies in the upper mantle based on inversion of only PP–P residuals. Violet lines indicate the main tectonic units, same as in Fig. 1. (For interpretation of the references to color in this figure legend, the reader is referred to the web version of this article.)

the models in Fig. 5, we can conclude that in the case of a sufficient amount of seismicity/stations in the study region, applying the PP–P scheme makes no sense. However, for the "blank" areas, this scheme seems to be one of the alternatives that allows closing the information gap, although qualitatively.

As we can conclude from the very low variance reduction (from 15 to 25%) in the PP–P data inversion, the noise level in these data is very high. In this case, the key test that allows us to estimate the contribution of the random noise is reconstruction with odd and even data. This test consists of a random separation of the entire dataset into two subsets (e.g., with odd and even numbers of rays) and in their independent inversions. For the Siberian region, the data amount in each window varied from ~3000 to ~8000, which is not very large. When these data are divided into two subsets, the statistical extraction of the coherent signal becomes more problematic. Therefore, to maintain stable results, for the halved datasets we implemented stronger damping than for the entire dataset. The results of the odd/even test presented in Fig. 6 show that the correlation of the obtained images is poor. In areas with low numbers of bounce points, such as in the Sayan region, the results do not fit with each other. In areas with sufficient information density, correlation is observed, although on a qualitative level. In deeper sections, the correlation is higher, mostly because large-scale anomalies dominate. This test shows that the results obtained using the PP–P scheme must be interpreted very carefully. In addition, we performed the odd/even test for the SS–S data and did not reveal any coherent signal. For the Ryukyu Arc (Western Pacific) where the subduction zone is clearly mapped by other methods, the SS–S data did not show any signature of the slab. We have concluded that the SS–S data are too noisy and not suitable for the tomographic inversion.

Synthetic tests are not the highest priority in this paper, but they form an important part for verification. All the presented synthetic tests were performed within a linear approach. The synthetic residuals were computed for the same rays as those used in real data inversion, computed in the 1D spherical model. The residuals were disturbed with random noise of 0.5 s of rms, which provided the same level of variance reduction (~20%) as in real data inversion. The statistical distribution of noise had a similar histogram to that of the observed residuals in the ISC catalogue. The reconstruction of the

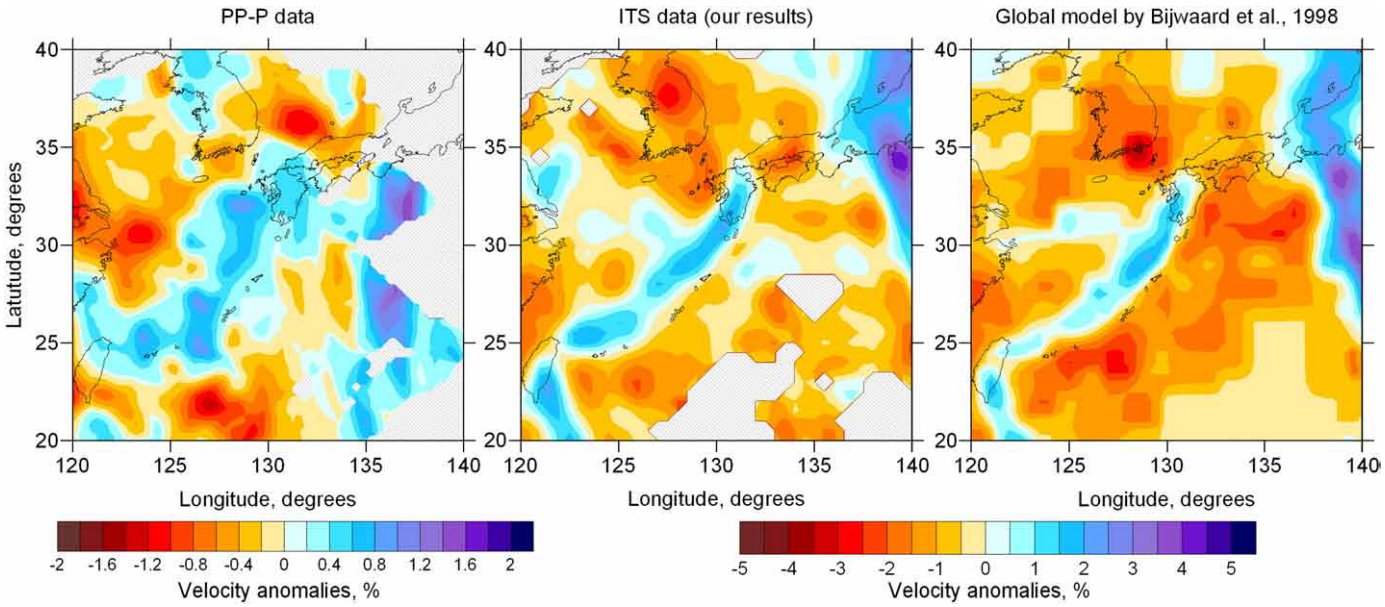

Fig. 5. Comparing the P-velocity structure beneath the Ryukyu Arc (Western Pacific) for the depth of 200 km obtained using different approaches: PP–P scheme (left); ITS scheme (center) and global ISC data inversion by Bijwaard et al., 1998 (right).

synthetic model was performed using the same grids and damping parameters as for the real data. The first test represents a single anomaly of 1% amplitude that changes the sign at a depth of 350 km (upper row in Fig. 7). It can be seen that the upper part of this anomaly is reconstructed robustly, while the lower part is restored with a significantly lower amplitude of perturbation. The second model (middle row in Fig. 7) represents alternating 300-km-wide anomalies. Vertically, the change of sign occurs at a depth of 350 km; the amplitudes of anomalies are 1%. It can be seen that in the northern part of the study area, in general, the anomalies are reconstructed correctly. However, they are strongly smeared in a diagonal direction, which can be explained by the dominant SE–NW orientation of the considered ray paths. In the southern part of the area, where less data is available, the 300-km anomalies are not resolved. The third test (lower row in Fig. 7) is similar to the second but with 600-km-wide anomalies. This configuration of the model is generally reconstructed correctly throughout the entire area, including the parts with lower density of information. As in the previous tests, the amplitudes of anomalies in the lower part are weaker than in the upper part. Synthetic modeling is also discussed in next sections when presenting the merged PP–P and ITS models.

5. Inversion according to the ITS scheme

In the southern mountains framing Siberia, there exists sufficient seismicity for us to apply the Inverse Tomographic Scheme (ITS). This scheme uses the travel times from events located in the study area that are recorded by worldwide stations at all available epicentral distances. The ITS has been applied to many different regions, including the Alpine-Himalayan belt (Koulakov et al., 2002), Pamir-Hindukush (Koulakov and Sobolev, 2006), Iran (Alinaghi et al., 2007), and Europe (Koulakov et al., 2009a). In this study, we use the same data that was used in Koulakov (2008) to investigate Southern Siberia and Mongolia. However, after publishing this paper, we further investigated the parameters of the inversion (e.g., grid spacing and damping parameters) to achieve a better resolution for the cases of synthetic and observed data inversions, so the model has changed slightly compared to the published version. The principle of data selection and inversion remains unchanged, so the technical details of the algorithm can be found in Koulakov (2008). We remind briefly that the inversion was performed in five circular overlapping windows of 7° radius and was then averaged into one model. In this study, inversion was applied with about 130,000 P arrivals from 1045 events in Southern Siberia and Mongolia. Fig. 8 shows the results for P velocity only.

For the models derived using the PP–P and ITS schemes, some correlations are observed on a qualitative level. The prominent pattern in both models is a dominating high-velocity anomaly beneath the Siberian craton at the depths of up to 200 km. To the south of the Siberian craton, the maximum of the low-velocity anomaly in both models coincides with the distribution of Cenozoic volcanism (see also Fig. 1). The difference between ITS and PP–P based models is mostly in the regions with low density of PP bounce points. It should be noted that the best correlation between the model is observed for the shallowest (50 km) and deepest (600) sections. At intermediate depth, the correlation is less evident, which may be due to the different vertical resolutions provided by the two schemes. In ITS, the rays use a wide range of epicentral distances that determine a variety of dipping angles of the rays, which is good for the vertical resolution. For the PP–P scheme, most of the rays correspond to teleseismic distances with steep incidence angles. Such rays cannot provide good vertical resolution.

6. Merging the results of the PP–P and ITS schemes

Initially, we planned to combine the data of the ITS and PP–P schemes and use them for a simultaneous inversion. However, realization of this approach failed. The problem is that the noise level in the PP–P data is significantly higher than for the ITS scheme. To overcome this noise in the PP–P scheme, we implement fairly strong damping, which stabilizes the solution and smoothes the model. If in the combined inversion we use damping adjusted for the ITS, in areas with dominant coverage by PP–P data, the solution oscillates due to noise. If we use strong damping adapted for the PP–P scheme, we lose relevant information in areas with good data coverage according to ITS. At the same time, we confess that a simultaneous inversion for P and PP–P data might be possible if these datasets are correctly weighted. However, we do not believe that there are systematic rules for finding best weights in this situation; thus their definition will be probably ad hoc and artificial.

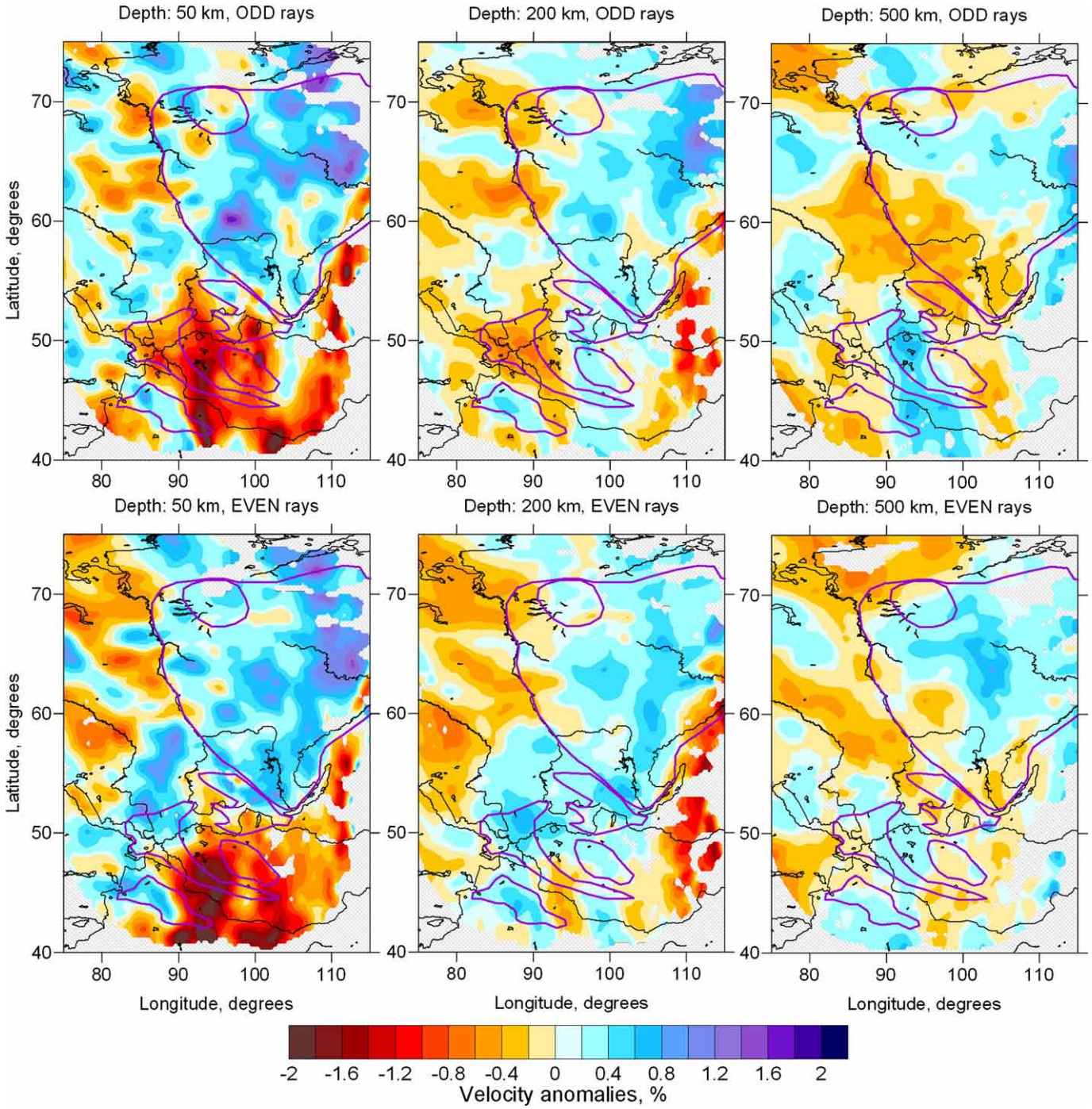

Fig. 6. Test with independent inversion of two randomly separated data subsets (PP–P pairs with odd and even numbers). Results for the depth of 50, 200 and 500 km are shown. Violet lines indicate the main tectonic units, same as in Fig. 1. (For interpretation of the references to color in this figure legend, the reader is referred to the web version of this article.)

As a result, we abandoned the idea of joint inversion and created a model based on merging the inversion results obtained independently using the PP–P and ITS schemes. A positive feature of this approach is a possibility to compare the independent results derived separately from both dataset in the overlapping areas. Combining the models, we took into account the varying reliability of both models in the study volume. As was mentioned above, for both the ITS and PP–P schemes the independent inversions are performed in a series of overlapping windows. In each window we performed the inversion for several differently oriented grids. To obtain the final velocity distribution, we merge all the models computed for different schemes, windows and grids. We define a special 3D weight function, shown in Fig. 9 which reflects the density of the parameterization nodes distributed according to the ray density. Formally for each scheme (ITS or PP–P), the weight function is written as:

$$W(x,y,z) = \frac{\sum_{\text{wind}} \sum_{\text{grid}} A_{\text{wind}} B_{\text{grid}}}{\sum_{\text{wind}} \sum_{\text{grid}} A_{\text{wind}}} \quad (1)$$

where A depends on the location of a current point with respect to the center of the current window and is equal to 1 in the center and 0 outside the window; and B depends on the distance to the nearest node of the parameterization grid and varies from 1 to 0. If the weight

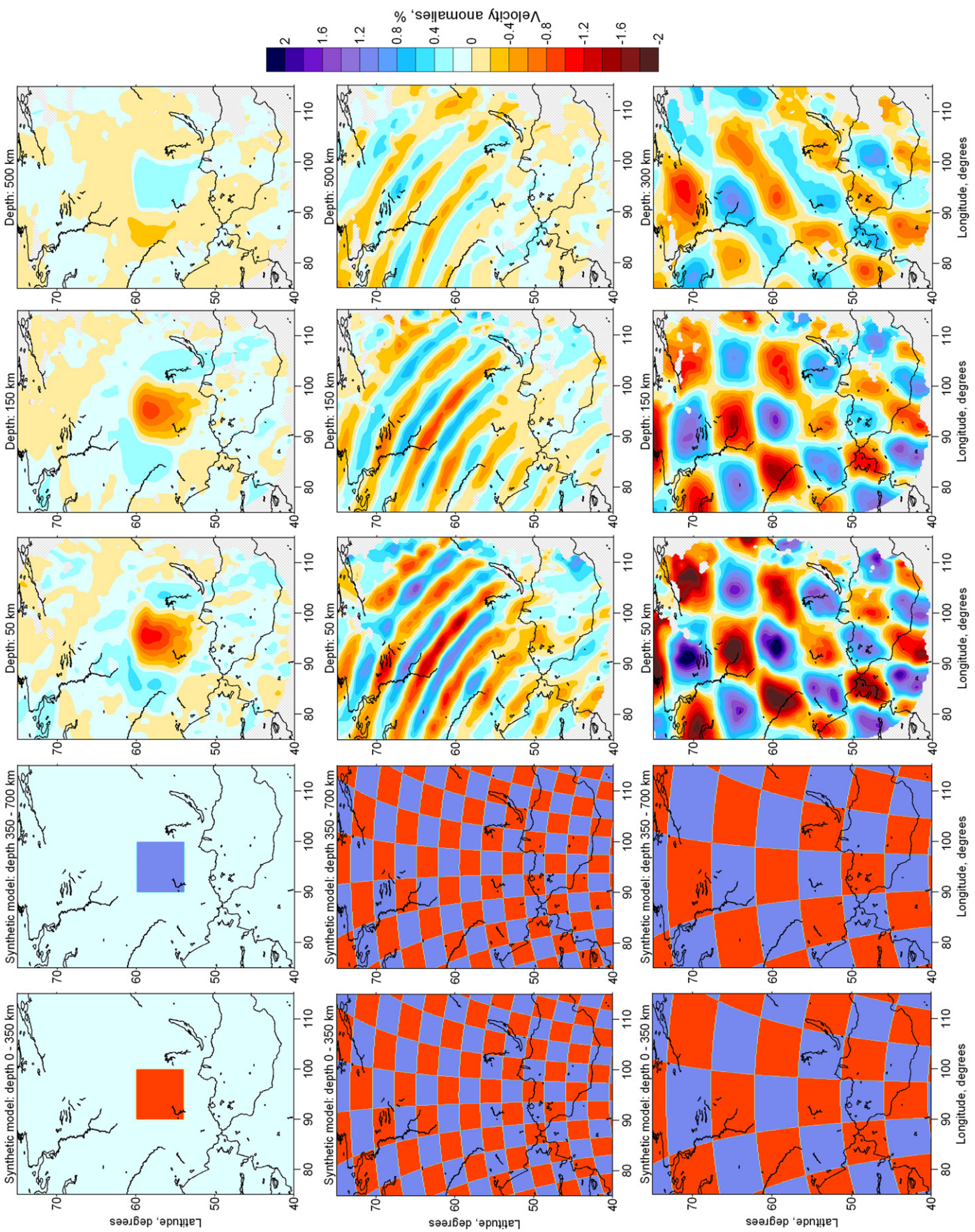

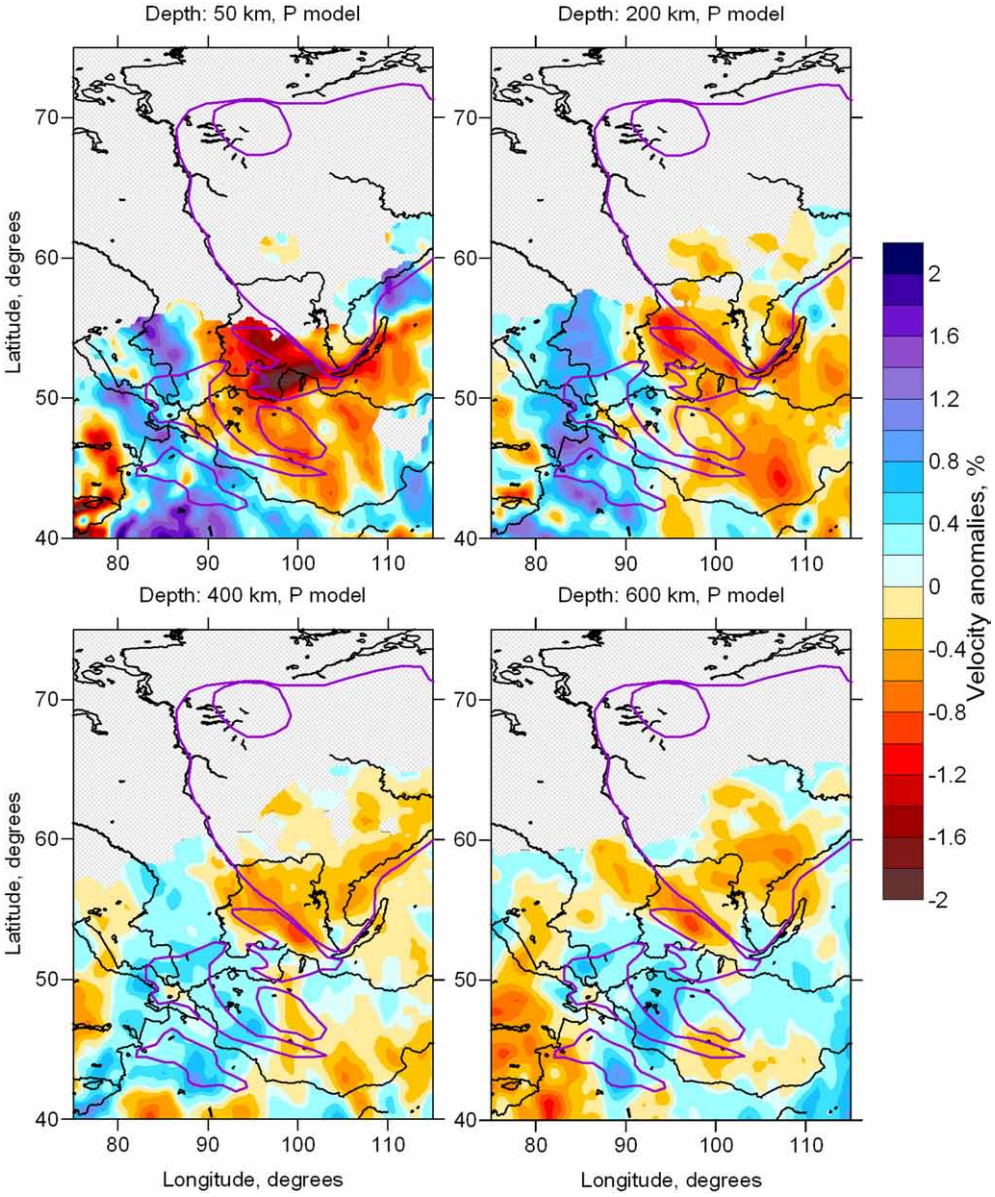

Fig. 8. Horizontal sections of the P-velocity anomalies obtained using the ITS scheme (sources in the study area recorded by the world wide stations). Violet lines indicate the main tectonic units, same as in Fig. 1. (For interpretation of the references to color in this figure legend, the reader is referred to the web version of this article.)

function is close to 1, in this point the density of information is high and it is more important for merging.

Merging of the results from different schemes is performed using:

$$dv = \frac{dv_{\mathrm{ppp}} K_{\mathrm{ppp}} W_{\mathrm{ppp}} + dv_{\mathrm{ITS}} K_{\mathrm{ITS}} W_{\mathrm{ITS}}}{K_{\mathrm{ppp}} W_{\mathrm{ppp}} + K_{\mathrm{ITS}} W_{\mathrm{ITS}}} \quad (2)$$

where dv_{its} and dv_{ppp} are values of velocity anomalies derived from the ITS and PP–P schemes, respectively. W_{its} and W_{ppp} are the weight functions computed using Eq. (1). K_{ppp} and K_{its} are the coefficients that reflect the significance of each scheme for merging. Their values are determined empirically. In the present case, $K_{ppp} = 0.5$ and $K_{its} = 1$. This means that if there is overlapping of the PP–P and ITS results, the results of the ITS would have two times higher priority. The results of merging are shown in four depth levels in Fig. 10 and in two vertical sections in Fig. 11.

For both the ITS and PP–P schemes we have computed several synthetic tests and merged them using the algorithm described above. Here we present two checkerboard tests with anomaly sizes of 300 and 600 km, the same as presented in Fig. 7. The noise level for the ITS was 0.3 s, while for the PP–P scheme it was 0.5 s. The merged model is presented in horizontal sections in Fig. 12. These tests demonstrate that adding the data according to the ITS scheme significantly improves the resolution in the southern part of the study area. At the same time, in areas lacking data for the ITS, the PP–P scheme provides robust images for the 600 km patterns.

7. Realistic synthetic model

A problem that is especially serious in the case of low quality data from the worldwide catalogues consists in the uncertainty of space resolution and amplitudes of the solution. The amplitude of the solution depends on many factors, the major one being the damping

Fig. 7. Three different checkerboard tests based on only PP–P data. Left two columns present the synthetic models in the depth interval of 0–350 km and 350–700 km. Right three columns are the reconstruction results at the depths of 50, 150 and 500 km.

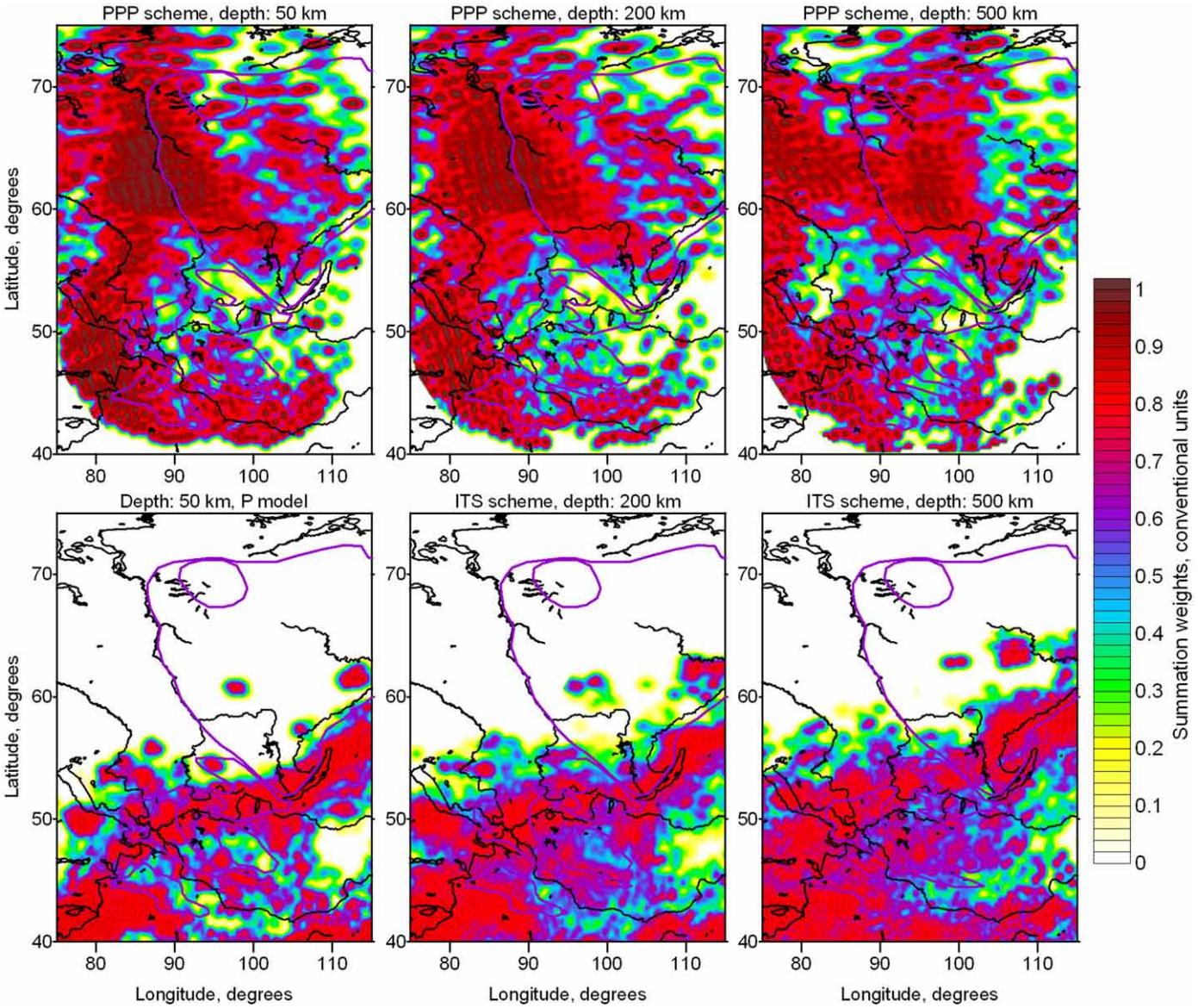

Fig. 9. Summation weights, in conventional units, which reflect the density of parameterization nodes for the models based on the PP–P (upper) and ITS (lower) schemes. See details in the text.

used for the matrix inversion. In the case of low quality data, as in this study, damping is determined by the noise level in the data. The stability of the solution is achieved by increasing the damping level. Therefore, the amplitude of the solution can be significantly different from the true value. Furthermore, the amplitude depends on the location of the anomaly and the ray coverage. This is clearly demonstrated by the synthetic tests presented in Section 3, where the deeper anomalies are generally weaker in amplitude than the shallower ones. Thus, as a rule, the solutions obtained after inversion of such inhomogeneous datasets provide usually only qualitative estimates for the real seismic distribution.

In order to evaluate realistic shapes and amplitudes of anomalies, we constructed an artificial model with a realistic velocity structure and used it to compute the synthetic times. Comparing the reconstruction results for the synthetic and real data allows us to make quantitative conclusions about parameters in the Earth. Tomography is like a photo camera with deformed and blurred lenses. It may perturb the shapes and amplitudes of patterns, and we should admit that the results of real data inversion are usually biased. We claim that if reconstruction results for real Earth and for synthetic model are similar, the distributions of velocities in the Earth are similar to the synthetic model. In this case, the synthetic model appears to be closer to the reality than the data inversion results. Such an approach of successive forward and inverse modeling has been applied for several observation schemes: in regional studies (e.g., Koulakov et al., 2009a, Europe), teleseismic tomography (e.g., Koulakov et al., 2006, Dead Sea Transform), local earthquake tomography (Koulakov et al., 2009b, Toba Caldera), and others.

Our synthetic model with realistic distributions of anomalies constrained after several trials is presented in horizontal sections (Fig. 13) and two vertical profiles (Fig. 11). The model anomalies are defined in a set of prisms. In map view each prism remains unchanged within a fixed depth interval. It should be noted that in constructing this artificial model, we took into account the existing a-priori information. The modeling with realistic synthetic anomalies allows us to check the credibility of existing geodynamical hypotheses. When computing the synthetic times, the random noise was added with rms of 0.6 s for the ITS and 0.9 s for the PP–P scheme.

Similarly as for the other tests described in Section 3, the forward and inverse modeling was performed within the linearized approach using the rays traced in the 1D model. As in the case of real data processing, the inversion was performed independently for the PP–P

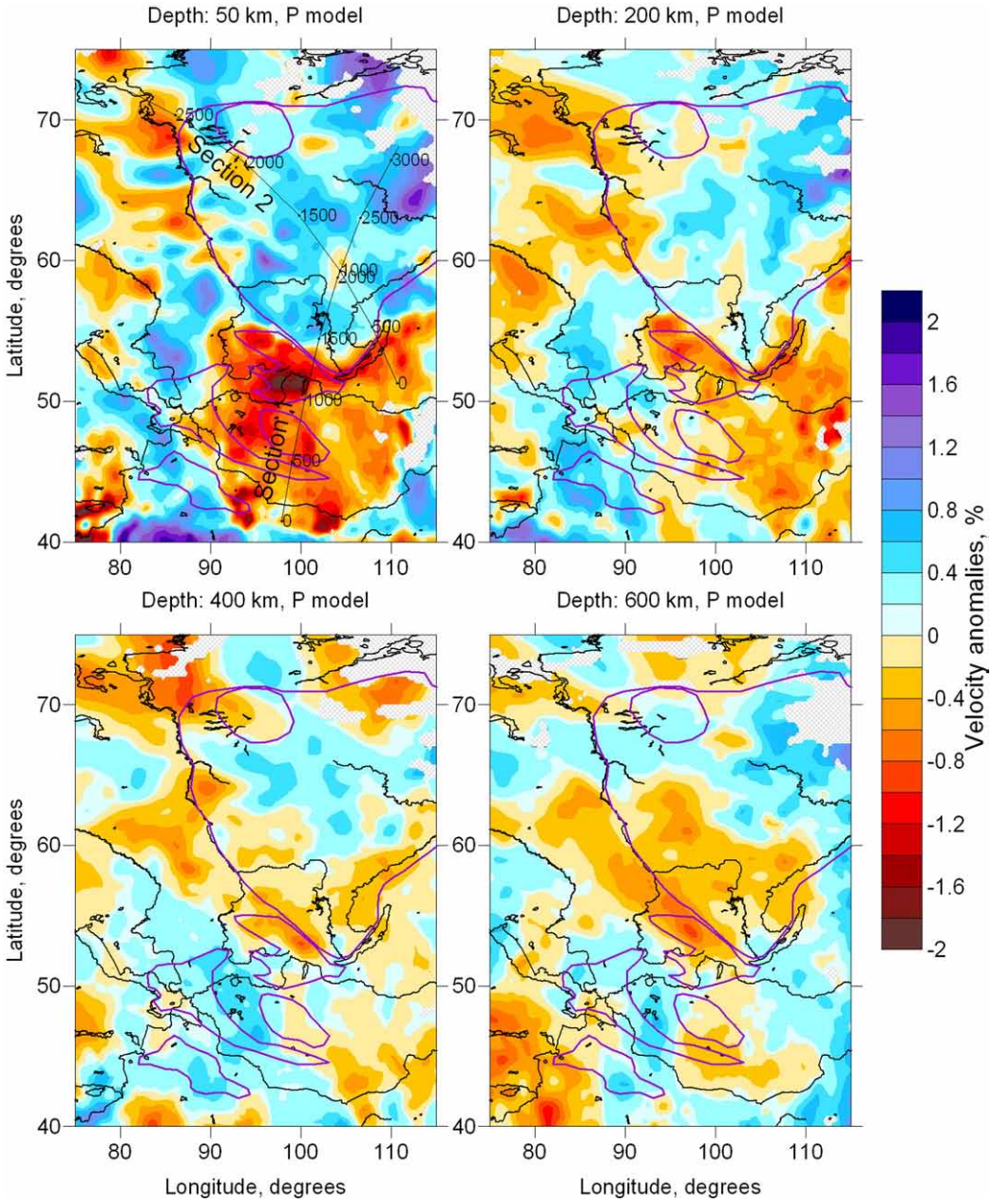

Fig. 10. Main result of this study: horizontal sections of P-velocity anomalies obtained as a result of merging the PP–P and ISC based models presented in Figs. 4 and 8, respectively taking into account weight functions in Fig. 9.

and ITS schemes, and the computed results were then merged in one model. All the inversion parameters (sizes and positions of the windows, grid spacing and orientations, damping, etc.) were identical as for the real data inversion. Amplitudes of anomalies in the artificial model were adjusted to achieve the best fit of the resolved amplitudes with the real data model.

The merged model for the reconstruction of the synthetic model using the PP–P and ITS schemes is shown in Figs. 11 and 13. The synthetic reconstructions in horizontal sections (Fig. 13) can be compared with the real data results presented at the same depths (Fig. 10). Vertical sections of the real data and synthetic models are shown in Fig. 11. We did not intend to achieve the same detailed elaboration as observed in the real data model. Thus, the reconstructed model seems to be smoother and simpler than the real data model. However, the models fit well with each other in both the amplitudes and the shapes of anomalies.

8. Discussion and interpretation

8.1. General remarks

The first observation that follows from the analysis of real data and synthetic model reconstructions is that the amplitudes of the retrieved anomalies were rather low. For example, for depths down to 200 km, the average contrast between the dominant positive and negative anomalies did not exceed 1.5%. However, for deeper sections, we estimated 0.5% and below. These results can be compared to tomographic models for other regions. The similar modeling of Europe (Koulakov et al., 2009a) has shown much larger velocity contrasts, including around 6% for 0–200 km depths and 2–3% for deeper sections. This may demonstrate that the intensity of mantle processes beneath the Siberian region and Mongolia is significantly weaker than in Europe. Another explanation could be insufficient resolution of the

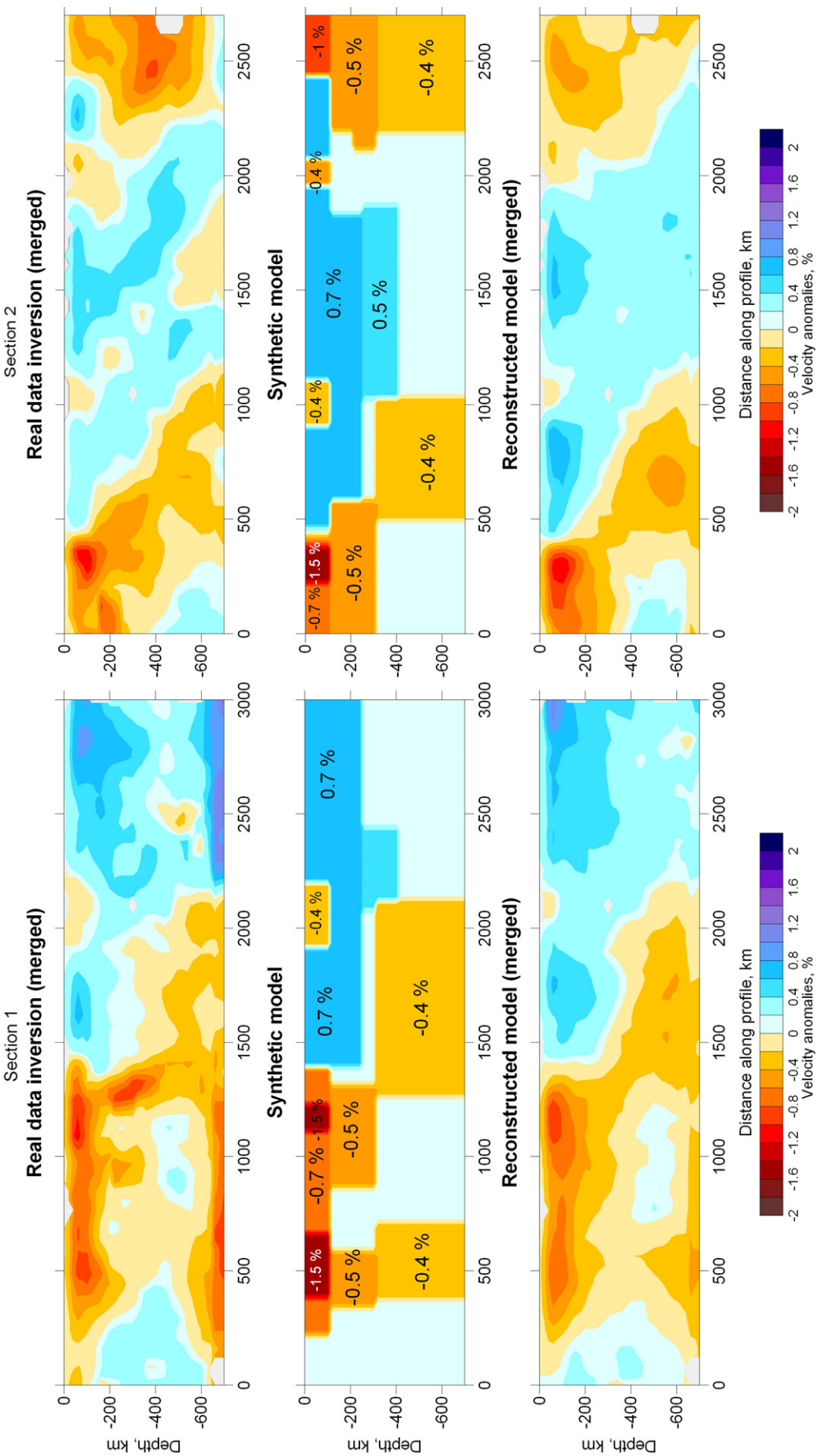

Fig. 11. Inversion results for real and synthetic data presented in two vertical sections indicated in Fig. 10 (50 km depth plot). Upper row represents the merged real data results, same as presented in Fig. 10. Middle row is the synthetic model, same as presented in Fig. 13. Numbers indicate the values of anomalies. Lower row is the result of reconstruction of the synthetic model using PP–P and ITS data, same as presented in Fig. 13.

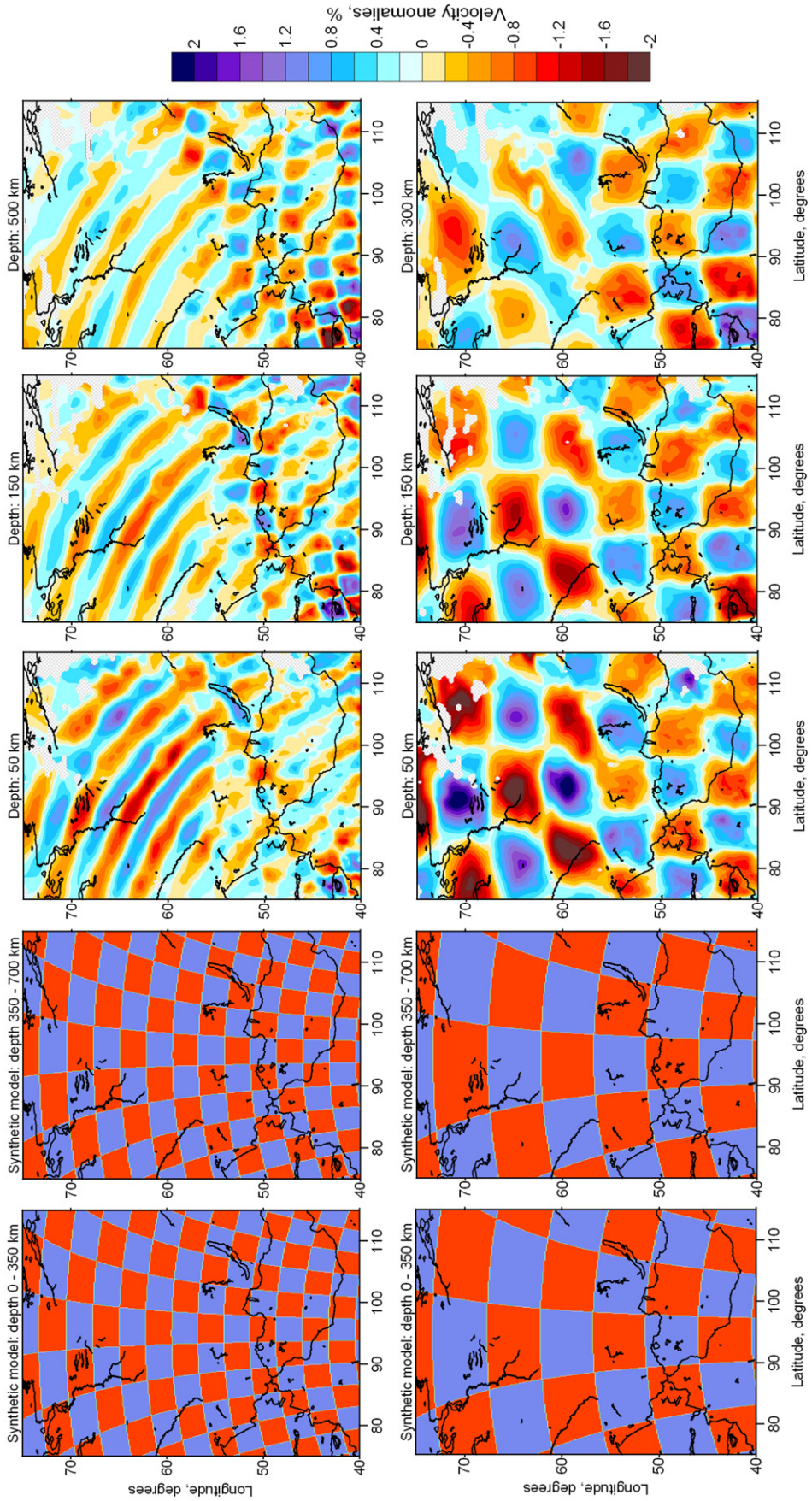

Fig. 12. Reconstructions of two checkerboard models obtained by merging the PP–P and ITS based results. Meaning of the plots are the same as in Fig. 7.

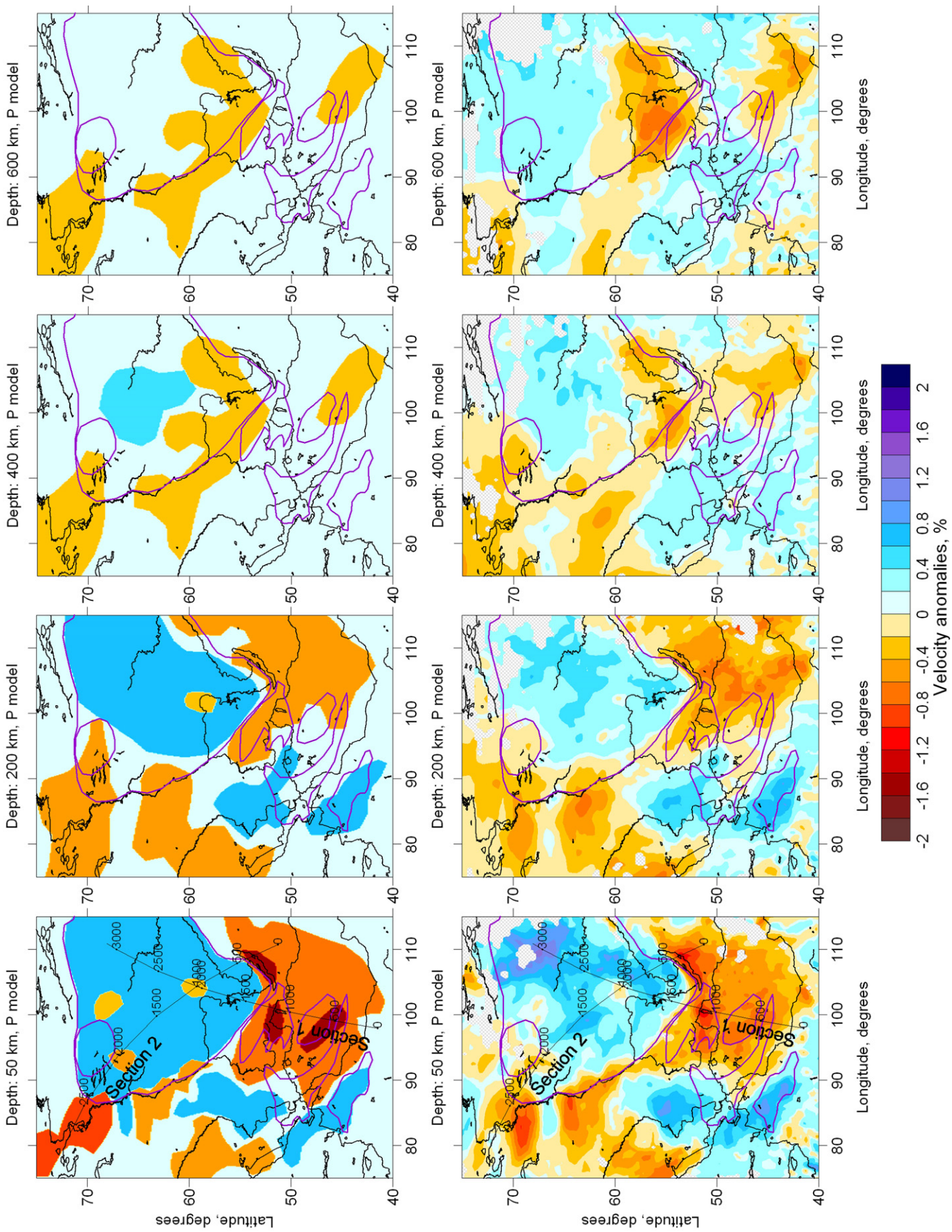

tomographic inversion in the present study. If tectonic processes are controlled by small-scale patterns in the upper mantle, even if they are highly contrasting (e.g., mantle plumes), then the reconstructed velocity model would be smooth and weak in amplitude.

Here we discuss the results of this and earlier studies and present our point of view on the role of mantle processes toward the geodynamical development of several units within the study region. We will consider three main topics. Two of these relate to processes in the southern mountain framing of Siberia. The third topic concerns the link between the mantle structure and regional geology of the two stable units in Northern Siberia, including the West Siberian Plate (WSP) and Siberian craton.

8.2. Relations to volcanic fields in Siberia and Mongolia

The mountains that frame Siberia to the south are located on the northern border of the Alpine-Himalayan orogenic belt. The geodynamical state of this area is controlled by both intra-plate interactions and mantle processes (e.g., Dobretsov et al., 1996). The manifestations of Cenozoic volcanism in Siberia and Mongolia are quite important. Logachev et al. (1996) and Logachev (2005) evaluated the total amount of Cenozoic erupted material in Southern Siberia and Mongolia as 6000 km^3. Roughly half of this amount corresponds to the Sayan area along the southern border of the Siberian craton. It is interesting that in Lake Baikal, which is the main rift depression of Siberia, no signature of Cenozoic volcanism has been observed (e.g., Eskin et al., 1978). Another volcanic field is related to the Hangay dome in Mongolia. Analysis of magma compositions in both areas has shown that they have generally similar properties (e.g., Yarmoluk et al., 1990), which probably indicates their common source. Rasskazov (1993) estimated the depth of their origin as 50–150 km, while the geochemical analysis by Ashepkov et al. (1996) provided an argument for a greater depth of the magma sources. Rasskazov et al. (1990) found a cyclic character in the volcanic activity, with the main maxima at 60, 30 and 10 Ma, as well as relatively quiet periods in between that lasted for 10–15 million years. The youngest manifestations of volcanism are observed in Eastern Sayan. Current volcanic activity seems to migrate to the N–W direction at an average rate of 0.9 cm/year (Rasskazov, 1994).

In our tomographic images, we observed a clear correlation between the Cenozoic volcanic fields (Figs. 1 and 10) and a regional scale low-velocity anomaly. This correlation was especially clear at shallower depths (50–100 km), where the amplitudes of anomalies beneath the volcanic areas reached 2%. For deeper sections, the anomalies were much weaker (approximately 0.5%) and displaced with respect to the volcanic fields.

The presence of several plumes beneath Mongolia and Southern Siberia, as well as their link with Cenozoic volcanism, was proposed by Zorin et al. (2002, 2003) based on long wave-length gravity anomalies. However, these individual plumes were not visible in the tomographic inversion results reported here and elsewhere. Koulakov (2008) explored a synthetic model, using the plume configuration from Zorin et al. (2002), and found that the resolution capacity of tomography is sufficient to resolve such kinds of patterns. If the data inversion does not provide any images of plumes, then either they do not exist, or they are much smaller than proposed by Zorin et al. (2002) and are not resolvable by tomography. Taking into account the deep nature of the magmas revealed by geochemistry studies (e.g., Ashepkov et al., 1996), we believe that the latter explanation is more probable. Thus, we propose the existence of several relatively small (less than 100 km in size) and highly contrasting channels (plumes) in the mantle that deliver overheated material to the volcanic fields. These are too small to be resolved by our tomographic scheme, but they could provide the general anomalous thermal background beneath Sayan and Mongolia that is observed in our tomograms as one regional low-velocity anomaly.

One of these plumes is probably located beneath the southern part of the Siberian craton. It was visible as a low-velocity anomaly in our tomograms at depths of 400 km and deeper. A similar feature was also observed in a global model by Gorbatov et al. (2001) and a regional teleseismic study by Zhao et al. (2006). This plume may accumulate hot material on the bottom of the cratonic lithosphere. While reaching a critical mass, this material starts moving up toward the border of the Siberian craton, where it produces fields of volcanic activity. This periodical process may explain the cyclic character of volcanic activity in Eastern Sayan (Rasskazov et al., 1990).

8.3. Baikal rift zone (BRZ)

One of the brightest features in the study area is the Baikal rift zone (BRZ), where regional extension resulted in the opening of a large depression that formed the Baikal Lake, as well as a series of other smaller rift basins. A long discussion about the origin of BRZ has continued for many years. An active mechanism of rifting that presumes the dominant role of asthenosphere upwelling (e.g., Logatchev et al., 1983) opposes the passive mechanism, in which the extension of BRZ is related to lithosphere plate interactions (e.g., Zonenshain and Savostin, 1981). The combined models also differ in the priority and role of mantle and lithospheric forces. For example, Petit et al. (1998) proposed the primary heating and weakening of the lithosphere by a mantle plume and subsequent concentrating of regional extensional forces in this weakened part. Other studies (e.g., Chemenda et al., 2002) have presumed that the primary concentration of an extension is due to local inhomogeneities in the lithosphere, which then cause a secondary asthenosphere upwelling.

In the first concept, the tomographic model presented in this study seems to be in favor with the active model of rifting in the BRZ. Indeed, beneath the entire Baikal rift zone we observed a large, low-velocity anomaly, which might represent the plume head or asthenosphere upwelling. This model seems to be consistent with the work of Rogozhina and Kozhevnikov (1979), who mapped the anomalous mantle area beneath the BRZ based on the delays of teleseismic rays at regional seismic stations. Our results are apparently consistent with teleseismic studies in the literature (Gao et al., 1997, 2003; Tiberi et al., 2003; Zhao et al., 2006). In these reports, a low-velocity anomaly was located beneath the BRZ at shallower depths, which then shifted toward the craton at greater depths. Similar conclusions followed from a multimode inversion of surface and S-wave forms in the Baikal area by Lebedev et al. (2006). All of these observations can be used as arguments for the major contribution of the active rifting mechanism in the BRZ.

At the same time, there are a number of counter arguments that do not corroborate the concept of an anomalous mantle beneath the BRZ. First of all, Jakovlev et al. (2007), who performed the tomographic inversion for the Baikal area based on *Pn* and *Sn* waves, did not detect a considerable velocity anomaly in the uppermost mantle beneath Baikal Lake and the eastern part of BRZ. On the other hand, they observed very bright low-velocity patterns beneath the S–W part of the BRZ that coincided with Cenozoic volcanic fields. Second, if the anomalous mantle played a considerable role in the opening of the crust, it would cause anomalous heating and volcanic processes (as in the East African Rift). In fact, we do not see any signature of Cenozoic volcanic activity in the Baikal basin (e.g., Eskin et al., 1978), which is the main argument against a mantle mechanism for the Baikal opening. It should be mentioned that Lysack (1992) observed anomalous heat flow in Baikal of up to 75–120 mW/m^2. However,

Fig. 13. Reconstruction of the synthetic model with realistic anomalies based on the results from the PP–P and ITS schemes. Upper row shows the shape of the 3D synthetic model in different depth levels; lower row is the reconstruction results (merged PP–P and ITS models).

these anomalies appear very local and seem to not represent a regional heating of the entire BRZ. Finally, receiver function studies performed independently by Zorin et al. (2002) and Gao et al. (2004) showed considerable variation in the Moho depth, from 40 km beneath the craton to 50–55 km beneath the eastern part of the BRZ. It is possible that the delays observed by Rogozhina and Kozhevnikov (1979) and the low-velocity anomaly beneath the BRZ in regional tomographic results are due to the effect of considerable (up to 10–15 km) crustal thickening. It is clear that, with the existing ray coverage, we cannot separate the crustal effect from the resulting velocity anomalies in the uppermost sections (probably up to 100 km in depth).

The low amplitudes of anomalies in the upper mantle beneath the study area may also indicate the minor effect of mantle processes on the intensive tectonic activity observed beneath Mongolia and the southern mountains framing Siberia. Anomalies of less than 1% in the mantle cannot represent a sufficiently powerful mantle circulation that is capable of causing rifting and regional mountain building processes. We conclude from this that active orogenesis in these areas is mostly due to the displacement and interaction of lithospheric plates driven from far away (e.g., the Indian plate indentor and Pacific subduction).

8.4. Siberian craton and West Siberian Plate

The Siberian craton is one of the largest Precambrian blocks that form the kernels of all continents on the Earth. The thick and cold lithosphere of most cratons is clearly mapped in all global tomographic models (e.g., Bijwaard et al., 1998; Gorbatov et al., 2001) as bright, high-velocity patterns. In our model, the Siberian craton was also robustly resolved as a dominant high-velocity anomaly within the boundaries indicated in tectonic maps. However, the structure of the craton was not homogeneous. Although the vertical resolution of the velocity anomalies was not good (especially for the PP–P scheme), a difference in the lithospheric thickness between the northern and southern segments of the Siberian craton can be identified (at least qualitatively). A high-velocity anomaly beneath the southern segment of the craton was observed down to about 200 km, which means that the lithosphere in that location is thinner. Beneath the northern segment (between 60° and 70° latitude), a high-velocity anomaly was observed at greater depths, which is evidence of a significantly thicker lithosphere. A similar feature was found in global tomographic models (e.g., Gorbatov et al., 2001). General heat flow background in the Siberian craton was about 30–40 mW/m^2 (Duchkov et al., 1987 and compilation in Bushenkova et al., 2002), which is a typically low value for Precambrian cratonic areas.

Inside the craton, several smaller scale seismic anomaly patterns seem to be robustly resolved in our model. One of these is a lower velocity pattern that was located in the crossing area of two profiles (Fig. 10). The reliability of this anomaly is supported by synthetic modeling with realistic anomalies (Figs. 11 and 13) and the odd/even test (Section 200 km in Fig. 6). In the vertical sections, this anomaly appears to be linked to a large low-velocity anomaly located beneath the southern segment of the Siberian craton. As was assumed in Section 8.2, this deep anomaly may feed the fields of basaltic volcanoes in Eastern Sayan along the southern perimeter of the Siberian craton. At the same time, the existence of local lower velocity anomalies inside the craton may indicate that the overheated material beneath the craton could also affect the cratonic lithosphere in some way (thermal and/or chemical). Above this pattern, Duchkov et al. (1987) observed a higher heat flow of about 45 mW/m^2.

The West Siberian Plate (WSP) is a large area located between the Russian and Siberian Precambrian cratons. Morphologically, the WSP is a very flat area where the elevation does not exceed 100 m. The N and NE segments of the WSP were formed during Paleozoic rifting, while its central and western segments originated from a Triassic rifting (Rudkevich, 1994). According to Ziegler (1992), the WSP was formed as a result of Permian–Triassic back arc extension in the Mesozoic period. Widespread basaltic volcanism occurred in the West Siberian Basin region 250 million years ago, which is synchronous with the bulk of the Siberian Traps that erupted further east on the Siberian Platform (Reichow et al., 2002).

Presently, the WSP is covered with a Mesozoic–Cenozoic sedimentary layer that was accumulated during a long and steady subsidence. The sedimentary cover has a maximal thickness of 8 km in northern areas and about 4 km in central parts (Rudkevich, 1994). This decreases toward the margins of the WSP. These sediments are objects of vital geophysical investigations, due to active oil and gas exploration in the WSP. The deep crustal and mantle structure has been studied along several transcontinental transects that used nuclear explosions as powerful sources of seismic signals (e.g., Pavlenkova et al., 1996; Egorkin, 1998; Morozova et al., 1999). According to these studies, the lithosphere thickness has been estimated at 150 km. Similar values were given by Artemieva and Mooney (2001) based on thermal lithospheric modeling.

Despite the absence of present day active tectonic processes and its quite homogeneous sedimentary cover, the deep structure of the WSP seems to be complicated and strongly heterogeneous. This is seen in the results of the abovementioned regional transects and in maps of the Moho and crystalline basement by Rudkevich (1994). In our tomographic images (Fig. 10), the upper mantle beneath the WSP appears to be quite heterogeneous. The obtained models show a clear separation between the high-velocity lithosphere of the Siberian craton and the lower velocities beneath Western Siberia. Beneath the WSP we observed quite strong velocity variations. It is interesting that the heat flow within the WSP (see the compilation heat flow map in Bushenkova et al., 2002, Fig. 10) varied considerably, from 45 to 70 mW/m^2, and that the main patterns of higher heat flow correlated with low-velocity anomalies in our tomograms.

We did not observe any correlation of our tomographic results with the distributions of the Siberian Traps and other igneous provinces in the WSP or Siberian craton. We believe that any signatures of processes in the mantle that were responsible for these eruptions disappeared completely or were replaced via convective mixing of the mantle beneath Siberia during several hundred million years.

9. Conclusions

In this study we found that PP–P differential residuals from the ISC catalogue are extremely noisy. In areas of good coverage with stations and/or earthquakes, the PP–P scheme based on these data cannot compete with the ITS and other body-wave tomographic schemes. However, in “blank” areas, where neither stations nor seismic events are available, the PP–P scheme can close the gap, although at a qualitative level. Taking into account the poor quality of the PP–P data, special attention must be paid to verifying the results. We present several tests aimed at revealing a coherent component if the noise level is stronger than the relevant signal. In this case, the most effective test is based on independent inversion of data subsets with odd and even numbers of rays. Based on different tests, we conclude that the SS–S data in the ISC catalogue are too noisy and cannot be used to retrieve any coherent result.

We have constructed a merged model for P-velocity anomalies in the upper mantle. In areas of good coverage with stations/events this model is mostly based on the ITS results. For the “blank” areas, the model is mostly based on the results of PP–P data inversion. For depths down to 200 km, we observe clear differentiation between high-velocity lithosphere of the Siberian craton and low-velocity anomalies beneath Mongolia and the mountains framing Siberia. The areas of Cenozoic basaltic volcanism in Sayan and Mongolia coincide with the locations of the strongest negative anomalies. At greater

depths, the most prominent low-velocity anomaly is located beneath the southern segment of the Siberian craton.

Beneath the Baikal rift zone we observe low-velocity anomaly which might be considered as an argument for the dominant role of a mantle mechanism in the rift opening (active rifting). However this anomaly can be due to considerable crustal thickening beneath the BRZ which is observed in receiver function studies. After analyzing all counter arguments we conclude that a passive mechanism which implies the dominant role of the lithosphere plate interactions is more probable for the BRZ.

Beneath the Western Siberian Plate, we observe fairly heterogeneous structure of velocity anomalies which correlate with the heat flow observations. We do not observe any correlation between the upper mantle structure and the distributions of large igneous provinces in Northern Siberia. We suppose that convectional mixing in the mantle lasted for several hundred million years erased any signatures of these events.

Relatively weak amplitudes of anomalies in the upper mantle beneath the study area (~1% only) probably indicate that regional tectonic processes in Southern Siberia and Mongolia are mostly caused by intra-plate interactions rather than mantle dynamics.

Acknowledgments

We are grateful to both anonymous reviewer and to Hans Thybo for very constructive criticism which helped us to improve the content of the paper. This study is supported by RFBR grant #s 08-05-00276-A and 08-05-00926-A, Heimholtz Society and RFBR joint research project 09-05-91321-SIG_a, multidisciplinary projects SB RAS 44, and project ONZ RAS 7.4.

References

Alekseev, A.S., Lavrentiev, M.M., Mukhometov, R.G., Neresov, N.L., Romanov, V.G., 1971. Numerical methods of investigation of the Earth's upper mantle structure. Mathematical Problems of Geophysics: Computer Center SB AS USSR, Novosibirsk, 2, pp. 143–165. [in Russian].

Alinaghi, A., Koulakov, I., Thybo, H., 2007. Seismic tomographic imaging of P- and S-waves velocity perturbations in the upper mantle beneath Iran. Geophys. J. Int. 169 (3), 1089–1102. doi:10.1111/j.1365-246X.2007.03317.x.

Artemieva, I.M., Mooney, W.D., 2001. Thermal thickness and evolution of Precambrian lithosphere: a global study. J. Geophys. Res. 106 (B8), 16387–16414.

Ashepkov, I.V., Litasov, Yu.D., Litasov, K.D., 1996. Garnet peridotite xenoliths from melanephelinites of Khentey range (South Baikal). Russ. Geol. Geophys. 37 (1), 130–147.

Barazangi, M., Ni, J., 1982. Velocities and propagation characteristics of *Pn* and *Sn* beneath the Himalayan arc and Tibetan Plateau: possible evidence for underthrusting of Indian continental lithosphere beneath Tibet. Geology 10, 179–185.

Bijwaard, H., Spakman, W., Engdahl, E.R., 1998. Closing the gap between regional and global travel time tomography. J. Geophys. Res. 103, 30,055–30,078.

Brandon, C., Romanowicz, B., 1986. A "no-lid" zone in the Central Chang-Thang platform of Tibet: evidence from pure path phase velocity measurements of long-period Rayleigh waves. J. Geophys. Res. 91, 6547–6564.

Bushenkova, N., Tychkov, S., Koulakov, I., 2002. Tomography on PP–P waves and its application for investigation of the upper mantle in Central Siberia. Tectonophysics 358, 57–76.

Chemenda, A., Deverchere, J., Calais, E., 2002. Three-dimensional laboratory modeling of rifting: application to the Baikal Rift, Russia. Tectonophysics 356, 253–273.

Darragh, R.B., 1985. Mapping of the upper mantle structure from differential (PP–P) travel time residuals. Phys. Earth. Plan. Int. 41 (1), 6–17.

Dobretsov, N.L., Buslov, M.M., Delvaux, D., Berzin, N.A., Ermikov, V.D., 1996. Mezo- and Cenozoic tectonics of the Central Asian mountain belt: effect of lithospheric plate interaction and mantle plume. Int. Geol. Rev. 38, 430–466.

Dricker, I.G., Roecker, S.W., 1994. Mapping of upper mantle shear wave velocity structure beneath Asia using SS–S data from Kirnos analog seismographs. Eos Trans. AGU 75, 464.

Dricker, I.G., Roecker, S.W., 2002. Lateral heterogeneity in the upper mantle beneath the Tibetan plateau and its surroundings from SS–S travel time residuals. J. Geophys. Res. 107 (B11), 2305. doi:10.1029/2001JB000797.

Duchkov, A.D., Lysak, S.V., Balobaev, V.T., et al., 1987. Heat field of the Siberian interior. Nauka, Novosibirsk, p. 197. in Russian.

Egorkin, A.V., 1998. Velocity structure, composition and discrimination of crustal provinces in the former Soviet Union. Tectonophysics 289, 395–404.

Eskin, A.C., Bukharov, A.A., Zorin, Yu.A., 1978. Cenozoic magmatism of Lake Baikal. Dokl. Akad. Nauk SSSR 239 (4), 926–929.

Friederich, W., 2003. The S-velocity structure of the East Asian mantle from inversion of shear and surface waveforms. Geophys. J. Int. 153, 88–102.

Fukao, Y., To, A., Obayashi, M., 2003. Whole mantle P wave tomography using P and PP–P data. J. Geophys. Res. 108 (B1), 2021. doi:10.1029/2001JB000989.

Gao, S., Davis, P., Liu, K., Slack, P., Rigor, A., Zorin, Y., Mordvinova, V., Kozhevnikov, V., Logatchev, N., 1997. SKS splitting beneath continental rift zones. J. Geophys. Res. 102, 22781–22797.

Gao, S.S., Liu, K.H., Davis, P.M., Slack, P.D., Zorin, Y.A., Mordvinova, V.V., Kozhevnikov, V.M., 2003. Evidence for small-scale mantle convection in the upper mantle beneath the Baikal rift. J. Geophys. Res. 108 (B4), 2194. doi:10.1029/2002JB002039.

Gao, S.S., Liu, K.H., Chen, C., 2004. Significant crustal thinning beneath the Baikal rift zone: new constraints from receiver function analysis. Geophys. Res. Lett. 31, L20610. doi:10.1029/2004GL020813.

Gobarenko, B.C., Yanovskaya, T.B., 1983. The study of the structure of horizontal heterogeneities in the upper mantle of the Altai-Sayan zone. Izv. Akad. Nauk SSSR, Ser. Fizika Zemli 4, 21–35.

Gorbatov, A., Fukao, Y., Widiyantoro, S., 2001. Application of a three-dimensional ray-tracing technique to global P, PP and Pdiff traveltime tomography. Geophys. J. Int. 583–593.

Grand, S.P., 1994. Mantle shear structure beneath the Americas and surrounding oceans. J. Geophys. Res. 99, 11,591–11,621.

Grand, S.P., van der Hilst, R.D., Widiyantoro, S., 1997. Global seismic tomography: a snapshot of convection in the Earth. GSA Today 7 (4), 1–7.

International Seismological Centre, 2001. Bulletin Disks 1–9 [CD-ROM], Internatl. Seis. Cent. Thatcham, United Kingdom.

Jakovlev, A., Koulakov, I., Tychkov, S.A., 2007. Moho depth and 3D velocity structure of the crust and uppermost mantle beneath the Baikal region from local tomography. Russ. Geol. Geophys. 48 (2), 204–220.

Kennett, B.L.N., Engdahl, E.R., Buland, R., 1995. Constraints on seismic velocities in the Earth from travel times. Geophys. J. Int. 122, 108–124.

Koulakov, I., 1999. Three-dimensional seismic heterogeneities beneath the Baikal area from local and regional tomography. Russ. Geol. Geophys. 40 (3), 317–333.

Koulakov, I., 2008. Upper mantle structure beneath Southern Siberia and Mongolia from regional tomography data. Russ. Geol. Geophys. 49 (3), 187–196.

Koulakov, I., Sobolev, S.V., 2006. A tomographic image of Indian lithosphere break-off beneath the Pamir Hindukush region. Geophys. J. Int. 164, 425–440.

Koulakov, I., Tychkov, S., Bushenkova, N., Vasilevskiy, A., 2002. Structure and dynamics of the upper mantle beneath the Alpine-Himalayan orogenic belt from teleseismic tomography. Tectonophysics 358, 77–96.

Koulakov, I., Sobolev, S.V., Weber, M., Oreshin, S., Wylegalla, K., Hofstetter, R., 2006. Teleseismic tomography reveals no signature of the Dead Sea Transform in the upper mantle structure. Earth Planet. Sci. Lett. 252 (1–2), 189–200.

Koulakov, I., Kaban, M.K., Tesauro, M., Cloetingh, S., 2009a. P and S velocity anomalies in the upper mantle beneath Europe from tomographic inversion of ISC data. Geophys. J. Int. 179 (1), 345–366. doi:10.1111/j.1365-246X.2009.04279.x.

Koulakov, I., Yudistira, T., Luehr, B.-G., Wandono, 2009b. P, S velocity and VP/VS ratio beneath the Toba caldera complex (Northern Sumatra) from local earthquake tomography. Geophys. J. Int. doi:10.1111/j.1365-246X.2009.04114.x.

Lebedev, S., Meier, T., van der Hilst, R.D., 2006. Asthenospheric flow and origin of volcanism in the Baikal Rift area. Earth Planet. Sci. Lett. 249, 415–424.

Li, C., van der Hilst, R.D., Engdahl, E.R., Burdick, S., 2008. A new global model for P wave speed variations in Earth's mantle. Geochem. Geophys. Geosyst. 9, Q05018. doi:10.1029/2007GC001806.

Logatchev, N.A., Zorin, Yu.A., Rogozhina, V.A., 1983. Baikal rift: active or passive? Comparison of the Baikal and Kenya rift zones. Tectonophysics 94, 223–240.

Logachev, N.A., 2005. History and geodynamics of the Baikal rift. In: Goldin, S.V., Mazukabzov, A.M., Seleznev, B.C. (Eds.), Actual Problems of Modern Geodynamics of Asia [in Russian]. Izd. SO RAN, Novosibirsk, pp. 9–32.

Logachev, N.A., Rasskazov, S.V., Ivanov, A.V., Levi, K.G., Bukharov, A.A., Kashik, S.A., Sherman, S.I., 1996. Cenozoic rifting in continental lithosphere. In: Logachev, N.A. (Ed.), Lithosphere of Central Asia [in Russian]. Nauka, Novosibirsk, pp. 57–80.

Lysack, S., 1992. Heat flow variations in continental rifts. Tectonophysics 208, 309–323.

Morozova, E., Morozov, I.B., Smithson, S.B., Solodilov, L.N., 1999. Heterogeneity of the uppermost mantle beneath Russian Eurasia from the ultra-long-range profile QUARTZ. J. Geophys. Res. 104 (B9) 20329-20248.

Ni, J., Barazangi, M., 1983. High-frequency seismic wave propagation beneath the Indian Shield, Himalayan Arc, Tibetan Plateau and surrounding regions: high uppermost mantle velocities and efficient *Sn* propagation beneath Tibet. Geophys. J. R. Astr. Soc. 72, 665–689.

Nolet, G., 1981. Linearized inversion of (teleseismic) data. In: Cassinis, R. (Ed.), The Solution of the Inverse Problem in Geophysical Interpretation. Plenum Press, pp. 9–37.

Paige, C.C., Saunders, M.A., 1982. LSQR: an algorithm for sparse linear equations and sparse least squares. ACM trans. Math. Soft. 8 (1), 43–71.

Pavlenkova, N.I., Pavlenkova, G.A., Solodilov, L.N., 1996. High velocities in the uppermost mantle of the Siberian craton. Tectonophysics 262, 51–65.

Petit, C., Koulakov, I., Devèrchere, J., 1998. Velocity structure around the Baikal rift from teleseismic and local earthquake traveltimes and geodynamic implications. Tectonophysics 296, 125–144.

Pines, I., Teng, T.-L., Rosenthal, R., Alexander, S., 1980. A surface wave dispersion study of the crustal and upper mantle structure of China. J. Geophys. Res. 85, 3829–3844.

Rasskazov, S.V., 1993. Magmatism of the Baikal rift zone. Nauka, Novosibirsk, p. 288. in Russian.

Rasskazov, S.V., 1994. Comparison of volcanism and recent hot spot structures in Yellowstone and Eastern Sayan. Russ. Geol. Geophys. 10, 67–74.

Rasskazov, S.V., Batymurzaev, A.S., Magomedov, Sh.A., 1990. Cycling of Cenozoic volcanism in South-western Prebaikal area. Russ. Geol. Geophys. 10, 64–72.

Reichow, M.K., Saunders, A.D., White, R.V., Pringle, M.S., Al'Mukhamedov, A.I., Medvedev, A.I., Kirda, N.P., 2002. $^{40}Ar/^{39}Ar$ dates from the West Siberian Basin: Siberian flood basalt province doubled. Science 296 (5574), 1846–1849. doi:10.1126/science.1071671.

Reichow, M.K., Saunders, A.D., White, R.V., Al'Mukhamedov, A.I., Medvedev, A.L., 2005. Geochemistry and petrogenesis of basalts from the West Siberian Basin: an extension of the Siberian Traps, Russia. Lithos 79, 425–452.

Ritzwoller, M.H., Levshin, A.L., 1998. Eurasian surface wave tomography: group velocities. J. Geophys. Res. 103, 4839–4878.

Ritzwoller, M.H., Barmin, M.P., Villasenor, A., Levshin, A.L., Engdahl, E.R., 2002. *Pn* and *Sn* tomography across Eurasia. Tectonophys. 358 (1–4), 39–55.

Rogozhina, V.A., Kozhevnikov, V.M., 1979. Anomaly mantle area beneath the Baikal rift. Novosibirsk, Nauka. 288 p.

Rudkevich, M.Y., 1994. Evolution of the West Siberian Basin. In: Roure, F., Ellouz, N., Shein, V.S., Skvortsov, I. (Eds.), Geodynamic Evolution of Sedimentary Basins, International Symposium. Editions TECHNIP, Moscow, pp. 123–134.

Surkov, V.S., 2002. Neogenean evolution of the young Ural-Siberian Platform. Russ. Geol. Geophys. 43 (8), 754–761.

Surkov, V.S., Lotyshev, V.I., 1989. Geophysical investigation of deep crustal structure of the Siberian Platform region. Explor. Geophys. 20, 39–42. doi:10.1071/EG989039.

Tiberi, C., Diament, M., Déverchère, J., Petit-Mariani, C., Mikhailov, V., Tikhotsky, S., Achauer, U., 2003. Deep structure of the Baikal rift zone revealed by joint inversion of gravity and seismology. J. Geophys. Res. 108 (B3), 2133. doi:10.1029/2002JB001880.

Tiberi, C., Deschamps, A., Déverchère, J., Petit, C., Perrot, J., Appriou, D., Mordvinova, V., Dugaarma, T., Ulzibaat, M., Artemiev, A.A., 2008. Asthenospheric imprints on the lithosphere in Central Mongolia and Southern Siberia from a joint inversion of gravity and seismology (MOBAL experiment). Geophys. J. Int. 175, 1283–1297. doi:10.1111/j.1365-246X.2008.03947.x.

van der Hilst, R.D., Engdahl, E.R., 1991. On ISC PP and pP data and their use in delay-time tomography of the Caribbean region. Geophys. J. Int. 106, 169–188.

van der Hilst, R.D., Widiyantoro, S., Engdahl, E.R., 1997. Evidence for deep mantle circulation from global tomography. Nature 386, 578–584.

van der Sluis, A., van der Vorst, H.A., 1987. Numerical solution of large, sparse linear algebraic systems arising from tomographic problems. In: Nolet, G. (Ed.), Seismic Tomography. Reidel, Dortrech, pp. 49–83.

Vasco, D.W., Johnson, L.R., Pulliam, J., 1995. Lateral variations in mantle velocity structure and discontinuities determined from P, PP, S, SS, and SS–S_dS travel time residuals. J. Geophys. Res. 100 (B12), 24,037–24,059.

Vasco, D.W., Johnson, L.R., 1998. Whole Earth structure estimated from seismic arrival times. J. Geophys. Res. 103 (B2), 2633–2671.

Villasenor, A., Ritzwoller, M.H., Levshin, A.L., Barmin, M.P., Engdahl, E.R., Spakman, W., Trampert, J., 2001. Shear velocity structure of central Eurasia from inversion of surface wave velocities. Phys. Earth Planet. Inter. 123, 169–184.

Widiyantoro, S., Gorbatov, A., Kennett, B., Fukao, Y., 2000. Improving global shear wave traveltime tomography using three-dimensional ray tracing and iterative inversion. Geophys. J. Int. 141, 747–758.

Woodward, R.L., Masters, G., 1991. Global upper mantle structure from long-period differential travel times. J. Geophys. Res. 96 (B4), 6351–6377.

Woodward, R.L., Molnar, P., 1995. Lateral heterogeneity in the upper mantle and SS–S traveltime intervals for SS rays reflected from the Tibetan Plateau and its surroundings. Earth Planet. Sci. Lett. 135, 139–148.

Wu, F.T., Levshin, A., 1994. Surface-wave group velocity tomography of East Asia. Phys. Earth Planet. Inter. 84, 59–77.

Wu, F.T., Levshin, A.L., Kozhevnikov, V.M., 1997. Rayleigh wave group velocity tomography of Siberia, China and the vicinity. Pure Appl. Geophys. 149, 447–473.

Yarmoluk, V.V., Kovalenko, V.I., Bogatikov, O.A., 1990. South-Baikal "hot spot" in the mantle and its role in development of the Baikal rift zone. Dokl. Akad. Nauk SSSR 312 (1), 187–191.

Zhao, D., Lei, J., Inoue, T., Yamada, A., Gao, S.S., 2006. Deep structure and origin of the Baikal rift zone. Earth Planet. Sci. Lett. 243, 681–691.

Ziegler, P.A., 1992. Plate tectonics, plate moving mechanisms and rifting. Tectonophysics 215, 9–34.

Zolotukhin, V.V., Al'Mukhamedov, A.I., 1988. Traps of the Siberian Platform. In: Macdougall, J.D. (Ed.), Continental Flood Basalts. Kluwer Academic, Amsterdam, pp. 273–310.

Zonenshain, L.P., Savostin, L.A., 1981. Geodynamics of the Baikal rift zone and plate tectonics. Tectonophysics 76, 1–46.

Zorin, Yu.A., Mordvinova, V.V., Turutanov, E.Kh., Belichenko, B.G., Artemyev, A.A., Kosarev, G.L., Gao, S.S., 2002. Low seismic velocity layers in the Earth's crust beneath Eastern Siberia (Russia) and Central Mongolia: receiver function data and their possible geological implication. Tectonophysics 359, 307–327.

Zorin, Y.A., Turutanov, E.Kh., Mordvinova, V.V., Kozhevnikov, V.M., Yanovskaya, T.B., Treussov, A.V., 2003. The Baikal rift zone: the effect of mantle plumes on older structure. Tectonophysics 271, 153–173.